Diffused sunlight driven highly synergistic pathway for complete mineralization of organic contaminants using reduced graphene oxide supported photocatalyst.

GANESH BABU, S., VINOTH, R., NEPPOLIAN, B., DIONYSIOU, D.D. and ASHOKKUMAR, M.

2015

Accepted Manuscript

Title: Diffused sunlight driven highly synergistic pathway for complete mineralization of organic contaminants using reduced graphene oxide supported photocatalyst

Author: Sundaram Ganesh Babu RamalingamVinoth Bernaurdshaw Neppolian Dionysios D. Dionysiou Muthupandian Ashokkumar

Please cite this article as: Sundaram Ganesh Babu, RamalingamVinoth, Bernaurdshaw Neppolian, Dionysios D.Dionysiou, Muthupandian Ashokkumar, Diffused sunlight driven highly synergistic pathway for complete mineralization of organic contaminants using reduced graphene oxide supported photocatalyst, Journal of Hazardous Materials http://dx.doi.org/10.1016/j.jhazmat.2015.02.071

Diffused sunlight driven highly synergistic pathway for complete mineralization of organic contaminants using reduced graphene oxide supported photocatalyst

Sundaram Ganesh Babu[a], RamalingamVinoth[a], Bernaurdshaw Neppolian[a,*], Dionysios D. Dionysiou[b], Muthupandian Ashokkumar[c]

[a] *SRM Research Institute, SRM University, Kattankulathur 603203, Chennai, Tamilnadu, India*

[b] *Environmental Engineering and Science Program, Department of Biomedical, Chemical and Environmental Engineering, University of Cincinnati, Cincinnati, OH 45221-0012, USA*

[c] *The School of Chemistry, University of Melbourne, Parkville, Melbourne, Victoria 3010, Australia*

* Corresponding Author. Tel.: +91-44-2741-7916; Fax: +91-44-2745-6702.
E-mail: neppolian.b@res.srmuniv.ac.in (B. Neppolian).

Graphical Abstract
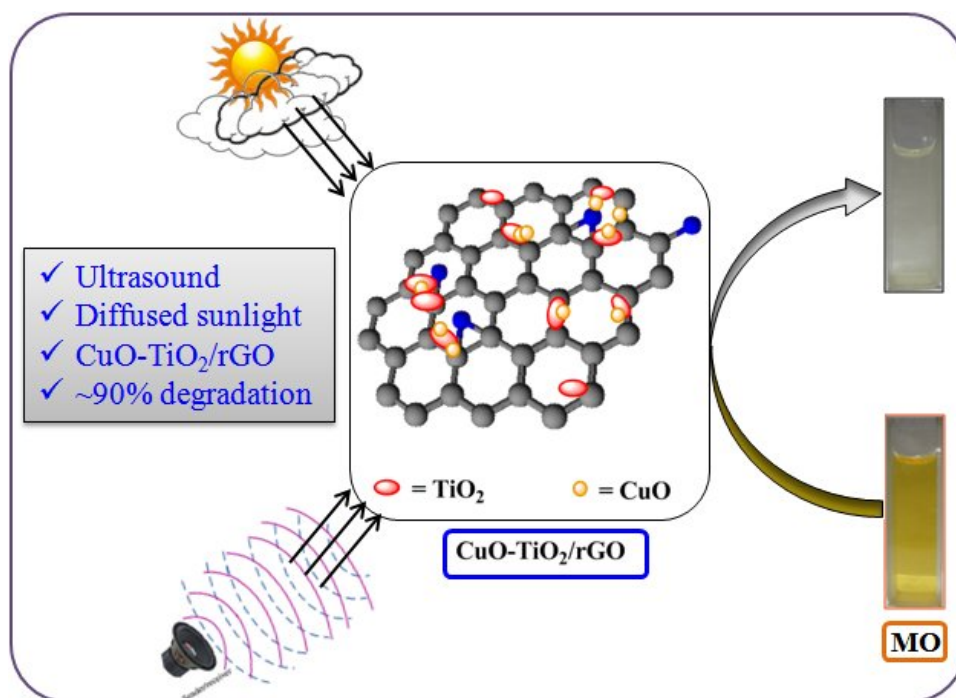
Highlights

- Diffused sunlight is firstly used as an effective source for degradation of organics

- More than10 fold synergistic effect is achieved by sono-photocatalysis

- rGO enhances the degradation efficiency up to 54% as compared with $CuO-TiO_2$ alone.

- Plausible mechanism and intermediates formed are supported with experimental studies

Abstract

Diffused sunlight is found to be an effective light source for the efficient degradation and mineralization of organic pollutant (methyl orange as a probe) by sono-photocatalytic degradation using reduced graphene oxide (rGO) supported $CuO-TiO_2$ photocatalyst. The prepared catalysts are characterized by XRD, XPS, UV-vis DRS, PL, photoelectrochemical, SEM-EDS and TEM. A 10 fold synergy is achieved for the first time by combining sonochemical and photocatalytic degradation under diffused sunlight. rGO loading augments the activity of bare $CuO-TiO_2$ more than two fold. The ability of rGO in storing, transferring, and shuttling electrons as well as the formation of heterojunction between TiO_2 and CuO facilitates the separation of photogenerated electron-hole pairs, as evidenced by the photoluminescence results. The complete mineralization of MO and the by-products within a short span of time is confirmed by TOC analysis. Further, hydroxyl radical mediated degradation under diffused sunlight is confirmed by LC-MS. This system shows similar activity for the degradation of methylene blue and 4-chlorophenol indicating the versatility of the catalyst for the degradation of various pollutants. This investigation is likely to open new possibilities for the development of highly efficient diffused sunlight driven TiO_2 based photocatalysts for the complete mineralization of organic contaminants.

Keywords: Diffused sunlight, $CuO-TiO_2$/rGO, Sonophotocatalysis, Synergistic effect, rGO.

1. Introduction

Photocatalytic degradation is a promising green route to convert organic pollutants from wastewater into harmless end products [1-6]. Initially, monometallic semiconducting oxides were exclusively studied for the photocatalytic degradation reactions [7-9]. By narrowing the band gap energy and thereby increasing absorption towards visible region of light, binary metal oxide composites were found to have better photocatalytic performance compared to single metal oxides, especially when visible light irradiation is used [10-12]. The major advantage of photocatalytic degradation is that it aims to use solar energy but most systems require ultraviolet light [13]. Nevertheless, the use of solar radiation as an energy source can reduce costs and also benefit the environment. Another major issue associated with photocatalysis is that strong adsorption of pollutants and their degradation products on the photocatalyst surface reduce the performance of catalysts. In addition, in the absence of vigorous stirring, catalyst particles settle down leading to a lower catalytic activity [14].

Ultrasound has also been widely used for chemical reactions, synthesis of nanomaterials, and oxidation of organic pollutants [15-17]. During ultrasonic irradiation of an aqueous solution, the cleavage of water molecules within cavitation bubbles leads to the formation of •H and •OH radicals. In oxygen rich solution, hydrogen atoms are converted into HOO• radicals, which are also powerful oxidants. The formed •OH and HOO• radicals are effective oxidizing agents to degrade organic pollutants in aqueous solutions [18]. The shear forces and shock waves generated during cavitation are useful for mass transfer leading to enhanced contact between the pollutant molecules and the catalyst particles. Therefore, ultrasound is successfully used in combination with other oxidation processes such as ozonation, Fenton, and Fenton-like methods [19]. Ultrasound with Fenton-like reagents has

5

shown synergistic effect for the degradation of pentachlorophenol [20], reactive blue 4 [15], methyl *tert*-butyl ether [21], *p*-chlorobenzoic acid [22], martius yellow [23] and also for the sonochemical oxidation of arsenic(III) to arsenic(V) [24]. Sonochemical degradation of organic pollutants in aqueous solutions is an effective method. However, the primary products generated are hydrophilic in nature and hence the mineralization of the pollutants and their degradation products is a very slow process.

The combination of both photocatalysis and sonochemical methods may overcome the existing problems of individual methods. A combination of both these advanced oxidation processes (AOPs) seems to enhance the degradation of organic pollutants due to increase in the amount of •OH radicals generated during the process [25]. However, most of the combined studies reveal an additive effect when combining photocatalytic reaction with ultrasound. Examples include the degradation of acid orange 8 and acid red 1 in waste water [26], azo dyes in presence of TiO_2 catalyst under UV light irradiation [27,28], and 4-chlorophenol with $Bi_2O_3/TiZrO_4$ [29].

In this study, methyl orange (MO) dye, which belongs to the class of azo dyes, was chosen as a target contaminants because it is very toxic, mutagenic, and carcinogenic [30-32]. The sonophotocatalytic degradation of MO with $CuO-TiO_2/rGO$ photocatalysts and the mechanism behind the observed synergistic effect under diffused sunlight are discussed in detail. To the best of our knowledge, this is the first study that reports on the significant synergistic effect of ultrasound combined with photocatalytic degradation of organic compounds under diffused sunlight.

6

2. Experimental methods

2.1. Preparation of Graphene Oxide (GO) and mesoporous TiO_2 NPs

Graphene oxide (GO) was prepared from graphite powder by modified Hummers' method using sodium nitrate, potassium permanganate, and sulphuric acid [33]. Mesoporous TiO_2 nanoparticles (NPs) were prepared by ultrasound-assisted method using titanium tetraisopropoxide (TTIP) and glacial acetic acid [34]. In a typical procedure, TTIP (0.032 mol) and glacial acetic acid (0.016 mol) were dissolved in 20 mL of absolute ethanol. The solution was stirred for 1 h and the resulting solution was added drop wise to 100 mL deionized water under sonication. The reactor was maintained at a constant temperature (30 °C) throughout the process with a water circulation jacket to avoid overheating. The suspension was sonicated for 3 h in pulse mode (3 s on and 1 s off, amplitude 40%) using a 13 mm diameter high intensity probe. After 3 h, the suspension was centrifuged, washed several times with water and dried in a hot air oven at 100 ºC for 2 h and then calcined at 400 ºC for 1 h to yield mesoporous TiO_2 NPs [35].

2.2. Preparation of CuO-TiO_2/rGO photocatalyst

Wet impregnation method was adopted for the synthesis of CuO-TiO_2/rGO photocatalyst (Fig. S1 in Supplementary Materials) [36]. Mesoporous TiO_2 NPs (300 mg) loaded onto GO (0, 1, 2 and 3 wt%) was dispersed in an appropriate concentration of aqueous solution (30 mL) of $Cu(NO_3)_2 \cdot 3H_2O$ (0, 0.5, 1.0, 1.5 and 2.0 wt% of Cu). In order to get effective impregnation, the solution was ultrasonicated for 10 min (20 kHz low frequency ultrasonicator). Then the mixture was pre-dried using a hot plate and the resultant powder was dried in an oven at 80 °C for 12 h and then calcined at 350 °C for 5 h.

7

2.3. Reactor set-up and analysis methods

In a typical procedure, 100 mg of CuO-TiO$_2$/rGO photocatalyst was dispersed in 100 mL of 10 mg/L MO solution (30 μM) in 150 mL reactor vessel. The mixture was magnetically stirred in dark for 40 min to reach adsorption equilibrium. Then the sonochemical reaction was carried out in the ultrasonic bath under diffused sunlight and the temperature of the bath was maintained at 30±3 ℃. At 20 min interval, 3 mL of dye solution was taken out and centrifuged at 10,000 rpm for 10 min to remove the residual CuO-TiO$_2$/rGO. The centrifuged samples were immediately analyzed using UV-vis spectrophotometer (Specord-200 plus UV-vis spectrophotometer, Germany) (Fig. 1a). As shown in Fig. 1b, the rate of mineralization was also monitored through Total Organic Carbon (TOC) analysis (Shimadzu TOC-L instrument, Japan). The sonophotocatalytic degradation of MO was evident to naked eye which is pictorially represented in Fig. 1c.

3. Results and discussion

3.1. Powder X-ray diffraction

X-ray diffraction analysis was carried out to identify the crystal structure and also to confirm the loading of CuO (Fig. 2). The XRD pattern confirmed the formation of only anatase phase of TiO$_2$ with reference to the JCPDS card number 21-1272 [37]. Resemblance of XRD pattern of TiO$_2$ in CuO-TiO$_2$ and CuO-TiO$_2$/rGO verified that no phase change occurred during the loading of CuO nanoparticles (NPs). In addition, CuO-TiO$_2$ and CuO-TiO$_2$/rGO showed significant peaks at 35.58, 37.10, 59.13 and 65.38º that correspond to the monoclinic crystal faces [(111), (111), (202) and (113)] of CuO (JCPDS card number 89-5895) [38,39]. This confirmed the presence of CuO NPs and TiO$_2$ in CuO-TiO$_2$/rGO photocatalyst. But there was not much difference between the XRD patterns of CuO-TiO$_2$

8

and CuO-TiO$_2$/rGO due to the fact that there were no structural/phase changes during the loading of GO.

3.2. X-ray photoelectron spectroscopy

XPS analysis was employed to identify the chemical oxidation states of Cu and Ti, and also to study the nature of oxygen functionalities in the catalyst. The survey spectrum clearly authenticated the presence of C 1s, O 1s, Cu 2p and Ti 2p peaks (Fig. S2a in Supplementary Materials). In order to determine the peak shift, curve fitting was performed by means of Gaussian−Lorentzian method. Before fitting the peaks, a Shirley baseline correction was made. The high resolution C 1s spectrum showed an asymmetric broad peak that suggested the existence of distinguishable carbons (Fig. S2b in Supplementary Materials). Deconvolution of C 1s peak gave five peaks with the binding energies at 284.4, 285.4, 286.8, 287.3 and 288.1 eV which correspond to C−C, C−OH, C−O−C, C=O and −COOH, respectively [40]. The oxygen functionalities, especially the epoxy group (C−O−C group), are able to reduce the carrier mobility over graphene layer and thereby may retard the photocatalytic activity. During ultrasound assisted synthesis followed by calcination at high temperature (350 ºC for 5 h), oxygen functional groups (epoxy groups) present in GO could be considerably removed, producing reduced GO (rGO) [41,42]. In the present case, oxygen functional groups were literally reduced during ultrasonication followed by calcination of the photocatalyst which was clearly evident from the low intense C=O, −COOH and C−O−C peaks. The O 1s spectrum was deconvoluted into three peaks (Fig. S2c in Supplementary Materials) [43]. The peak at 530.0 eV was ascribed to C=O and/or Ti−O−Ti and the peak at 530.9 eV was due to the residual −COOH and/or O=C−O−Ti. Likewise the C−O−C and/or Ti−OH functionalities were observed at 532.0 eV [44]. Similarly, the high resolution Cu 2p

9

region showed two major peaks at 942.0 and 961.0 eV which were attributed to the Cu $2p_{3/2}$ and Cu $2p_{1/2}$, respectively [45]. Furthermore, the shake-up satellite peaks of Cu $2p_{3/2}$ and Cu $2p_{1/2}$ were observed at 951.0 and 970.0 eV (~9 eV higher than the corresponding main peaks). Indeed, the shake-up satellite is a characteristic peak for CuO owing to d^9 configuration of ground state of Cu. On the other hand, the satellite peaks were absent for Cu_2O because the d shell is completely filled and hence the screening *via* a charge transfer into the d states is not possible. Therefore the appearance of the shake-up satellite peaks confirmed the formation of CuO (Fig. 3a) [46]. Likewise, the Ti 2p region illustrated two representative peaks at 458.6 and 467.5 eV which are attributed to Ti $2p_{1/2}$ and Ti $2p_{3/2}$, respectively. In addition to these, two more peaks at 459.4 and 469.8 eV were observed in Ti 2p high resolution region that correspond to the Ti−C bond (Fig. 3b). It is worth to mention here that the values are in agreement with those reported in the literature and confirmed the presence of TiO_2 [47].

3.3. UV-vis DRS

TiO_2, CuO-TiO_2 and CuO-TiO_2/rGO were analyzed by UV-vis DRS and the corresponding Tauc graphs were plotted to calculate the band gap energies (Fig. 4). The nature of absorption band with a sharp 'cut-off' at 384 nm was assigned to the phase pure TiO_2 (Fig. 4a) which corresponds to a band gap of 3.23 eV (Fig. 4b) [48]. The absorption edge of TiO_2 was slightly extended to the visible light region (403 nm and band gap energy, $E_{bg} = 3.08$ eV) with CuONPs (Fig. 4c). A similar trend was observed with Ag doped TiO_2 by Lalitha et al [49]. Furthermore, the band gap energy remained the same even after loading CuO-TiO_2 nanocomposites over rGO layer (Fig. 4d). This result suggests that rGO was present only as a solid support and did not alter the band gap of CuO-TiO_2 photocatalyst.

3.4. SEM-EDS

SEM-EDS analysis was carried out to study the surface topography and the corresponding elemental weight percentage of the CuO-TiO$_2$/rGO photocatalyst (Fig. S3 in Supplementary Materials). The spherical structure of mesoporous TiO$_2$ NPs can be clearly observed from the SEM images recorded at 3 μm (Fig. S3a in Supplementary Materials) and 1 μm (Fig. S3b in Supplementary Materials) scales. In addition, tiny secondary particles found on the surfaces of TiO$_2$ might be due to CuO NPs. The purity of CuO-TiO$_2$/rGO photocatalyst was examined by EDS analysis which showed the presence of only carbon, oxygen, copper and titanium elements.

3.5. TEM

Fig. 5 shows TEM images and the crystallite size distribution of CuO-TiO$_2$/rGO photocatalyst. The TEM images clearly reveal that CuO-TiO$_2$ nanocomposites are well distributed over rGO layer (Fig. 5a). Fig. 5b confirms that CuO-TiO$_2$/rGO possesses distorted elliptical and spherical structures with narrow range of particle sizes. Crystal size distribution graph discloses the particle size distribution of CuO-TiO$_2$/rGO ranging from 10 to 16 nm with an average of 13 nm (Fig. 5c).

3.6. Photoluminescence and photoelectrochemical studies

To characterise the photoexcited electron-hole pairs, photoluminescence (PL) spectroscopic analysis was carried out for mesoporous TiO$_2$ NPs, TiO$_2$/rGO, CuO-TiO$_2$, CuO/rGO and CuO-TiO$_2$/rGO (Fig. 6a). All the photocatalysts except CuO/rGO photocatalyst showed similar PL spectrum with three emission peaks located at 437, 469 and 493 nm. The PL peaks at 437 and 469 nm are owing to the band edge free excitons. Similarly

11

the excitonic PL signal centered at 493 nm is directly related to surface oxygen vacancies or defects in the photocatalysts. As seen from Fig. 6a, the luminescence intensity of bare TiO_2 was very high as compared to all other composites which indicated the highest radiative recombination rate of electron-hole pairs in bare TiO_2. The PL intensity of $CuO-TiO_2$ is slightly lower than that of TiO_2/rGO photocatalyst. This is due to the fact that the conduction band energy levels of CuO and TiO_2 are well matched with each other which facilitates fast transport of electrons and thereby hinders the rate of charge carrier recombination. In addition, it is interesting to note that the luminescence intensity of $CuO-TiO_2/rGO$ photocatalyst is remarkably lower than the luminescence intensities of $CuO-TiO_2$ and TiO_2/rGO photocatalysts. Thus, rGO not only acts as a potential solid support but also efficiently separates the photoexcited electron-hole pairs at $CuO-TiO_2$ interfaces [50]. Generally, electrons tend to move from higher Fermi energy level to lower Fermi energy level to adjust the energy level of electronic states [51]. As reported earlier, the conduction band (CB) work function of rGO is less than that of TiO_2 [52]. Hence, the electrons from TiO_2 easily transferred to rGO sheet and subsequently to CuO which further inhibited the recombination and thereby enhanced the carrier separation.

Photoelectrical response of TiO_2, $CuO-TiO_2$ and $CuO-TiO_2/rGO$ were studied in order to validate the role of rGO in transferring electron form TiO_2 to CuO (Fig. 6b). It is clearly evident from the photocurrent measurements that the $CuO-TiO_2/rGO$ generates higher photocurrent than that of bare TiO_2 and $CuO-TiO_2$. The photocurrent enhancement of $CuO-TiO_2/rGO$ photocatalyst confirmed the prevention of charge carrier (electron-hole pair) recombination. This further authenticated that rGO act as a potent carrier mobile layer at the CuO and TiO_2 heterojunction.

12

3.7. Catalytic efficiency

Initially, the sonophotocatalytic degradation of MO was compared with prepared catalysts: TiO_2-rGO, CuO-rGO, CuO-TiO_2 without rGO and with rGO as CuO-TiO_2/rGO in order to understand the specific roles of TiO_2, CuO and rGO in the CuO-TiO_2/rGO and the results are shown in Fig. 7. It can be seen that the % degradation of the dye is insignificant in all cases except in the case of sonophotocatalytic degradation using CuO-TiO_2/rGO (Fig. 7) and a similar trend is observed with TOC results (% mineralization). This observation emphasized the importance of TiO_2, CuO and rGO for MO degradation. The relative order of activities towards the photocatalytic degradation of MO under diffused sunlight combined with ultrasound is: CuO-TiO_2/rGO > CuO-TiO_2 > CuO/rGO > TiO_2/rGO > meso-TiO_2 NPs. As per Fig. 7, almost similar sonophotocatlytic activity was observed with CuO-TiO_2 and TiO_2/rGO photocatalysts which inferred that presence of either co-catalyst (CuO) or carrier transport layer (rGO) suppressed the electron-hole pair recombination rate in TiO_2. Moreover, it is interesting to observe that CuO/rGO (without TiO_2) photocatalyst also showed notable degradation under similar experimental conditions which suggests that the photogenerated holes (h^+) from CuO generated •OH radicals over rGO surface for the degradation of MO.

3.8. Effect of amount of GO and Cu loading

The results discussed above showed only ~35% degradation by CuO-TiO_2 (without rGO), whereas rGO loaded CuO-TiO_2 catalyst caused 89% degradation highlighting the influence of rGO in the present catalytic system. The increased photocatalytic performance of rGO loaded photocatalyst is well supported by the effective charge carrier separation in CuO-TiO_2/rGO photocatalyst, as evident from the photolumniesence (Fig. 6a) and photocurrent

results (Fig. 6b). To find out the optimal amount of rGO support, experiments were performed by varying the amount of rGO with fixed $CuO-TiO_2$ (Fig. S4a in Supplementary Materials). GO loading was varied in the range 0, 1, 2 and 3% with respect to $CuO-TiO_2$ content and the corresponding MO degradation was found to be 35, 54, 89 and 41%, respectively. The maximum catalytic activity was obtained with 2 wt% GO loading. However, further increase in GO loading (3% GO) decreased the efficiency of the catalyst. This could be due to the fact that increased GO loading can mask or prevent the direct contact between the light and the catalyst's surface. Therefore, 2 wt% of rGO was fixed for the rest of the experimental studies.

Similarly, the specific influence of CuO on the sonophotocatalytic degradation of MO under the diffused sunlight was studied with different CuO loading (0 – 2.0 wt%) with TiO_2/rGO because the photogenerated electrons migrate from TiO_2 to CuO through rGO. As mentioned earlier, without CuO, a negligible sonophotocatalytic reaction was noted under the diffused light. With the initial increase of Cu loading (0, 0.5, 1.0 and 1.5 wt%), the MO degradation also increased gradually (35, 43, 80 and 89%, respectively) and exhibited a maximum efficiency with 1.5% Cu loaded catalyst (Fig. S4b in Supplementary Materials). This is similar to previous observations reported by many researchers on the doping of metals on TiO_2, where around 1 wt% metal showed a maximum reactivity [53]. This might be due to the fact that Cu loading (1.5%) caused a shift in the effective band gap energy from 3.23 eV to 3.08 eV (Fig. 4). Further increase of Cu loading (2% Cu) had no much influence on the photocatalytic performance towards MO degradation. Hence 1.5% Cu loaded photocatalyst [$CuO-TiO_2$/rGO (1.5% Cu and 2% rGO)] was used as an optimal amount for the photocatalytic degradation of MO in sonophotocatalytic degradation under diffused sunlight.

14

3.9. Photo-, sono- and sono-photocatalytic degradation of MO

The sonophotocatalytic degradation efficiency of the optimized catalyst under the irradiation of diffused sunlight was evaluated using MO. For comparison, sonochemical and photocatalytic degradation studies were performed and the results are shown in Fig. 8. When the experiments were carried out in dark with ultrasound only and under diffused sunlight in the absence of ultrasound, the percentage degradations were 3.2 and 5.7, respectively. Interestingly, the reaction under diffused sunlight along with ultrasonication in the presence of $CuO-TiO_2/rGO$ showed a remarkable effect on the percentage degradation (up to 89%) of MO in 120 min (Fig. 8). The corresponding calculated synergistic effect is 10 fold (see Supplementary Materials, equation S1-S4) which is a very high significant; such high synergistic effect has not been reported in previous studies. This synergistic effect of ultrasound on photocatalytic degradation can be attributed mainly due to the presence of $CuO-TiO_2/rGO$ photocatalyst. As it was explained earlier, the synergistic effect observed is around 1 to 1.5 in the case of heterogeneous photocatalysis coupled with ultrasound [54]. Those reactions mostly employed powerful germicidal UV light irradiation (254 nm) or direct sunlight as a source of irradiation. However, only diffused sunlight was used as a source of irradiation in the present study. It is interesting to note that a similar enhancement effect was observed for the total mineralization of the dye. Thus, this coupled method may open up a new area of research not only for the degradation of organics but also for the synthesis of organic compounds. In order to illustrate the generality of this novel diffused sunlight driven sonophotocatalytic degradation process, degradation of another organic dye namely, methylene blue (MB) was investigated (Fig. 9a). Complete degradation of MB was observed within 100 min using the optimized $CuO-TiO_2/rGO$ catalyst. Furthermore, the effectiveness

of the proposed degradation route using CuO-TiO$_2$/rGO catalyst was tested with 4-chlorophenol apart from MO and MB (Fig. 9b). A similar trend was observed for both degradation and mineralization of 4-chlorophenol and thus, the catalyst is proved to be effective for the degradation of different types of organic pollutants.

3.10. Reusability

The lifetime of the photocatalyst (durability) and its level of reusability are very important characteristics. To verify the reusability of the photocatalyst, MO degradation was studied with 0.02 mM in presence of 100 mg of CuO-TiO$_2$/rGO using ultrasonic irradiation under diffused sunlight (Fig. S15b in Supplementary Materials). After completion of the reaction, the photocatalyst was separated by centrifugation and washed with water and dried at 80 ºC for 2 h and then used for further tests. For all the three cycles, level of degradation was consistently observed as 99% after 100 min under identical experimental conditions. This is clear indication that the catalysts can be reused for more number of times without losing its catalytic activity.

3.11. Proposed sonophotocatalytic degradation pathway

In order to confirm whether this sonophotocatalytic pathway proceeded *via* the degradation of MO by •OH radicals or merely by the adsorption of MO over the surface of photocatalyst under the diffused sunlight, LC-MS analysis was carried out. The chromatograms of MO were recorded after 0, 20, 60 and 120 min of sonophotocatalysis using CuO-TiO$_2$ and CuO-TiO$_2$/rGO photocatalysts (Fig. S7a−b in Supplementary Materials). The chromatograms clearly show the appearance of peaks corresponding to the degradation products. The components eluted at different retention time were subjected to mass

16

spectrometry and the structures of by-products were identified by interpretation of their fragment ions in the mass spectra (Fig. S8-S14 in Supplementary Materials). The LC-MS data suggest that certain amount of MO ($m/z = 304$) was degraded to products with m/z values of 210, 215, 290 and 313 using the CuO-TiO$_2$ photocatalyst. The presence of rGO enhanced the photocatalytic performance which was apparent by the complete sonophotocatalytic degradation of MO in presence of CuO-TiO$_2$/rGO photocatalyst. It is worth to mention that even the peak areas of the by-products were also very low in the case of CuO-TiO$_2$/rGO system. This suggests that CuO-TiO$_2$/rGO photocatalyst not only degraded the MO completely but also degraded the products evolved during sonophotocatalytic degradation process. These chromatographic results also suggested the complete mineralization of MO under the diffused sunlight driven sonophotocatalytic technique using CuO-TiO$_2$/rGO, which is in good agreement with the TOC results (Fig. 1b). Based on the m/z value structure of the products formed from MO during the sonophotocatalytic degradation using CuO-TiO$_2$ (Scheme 1) and CuO-TiO$_2$/rGO (Scheme 2) were determined [55]. These results suggested that the •OH radicals produced from diffused sunlight is sufficient for the complete sonophotocatalytic degradation of MO.

3.12. Plausible mechanism

Based on the observations, a plausible mechanism is proposed for the degradation of MO using CuO-TiO$_2$/rGO photocatalyst in sonophotocatalytic method under diffused sunlight as shown in Fig. 10. Around 5% UV light present in sunlight excites the electrons (e$^-$) from the valence band (VB) of TiO$_2$ to the conduction band (CB) and leaving h$^+$ in the VB. This leads to the formation of e$^-$–h$^+$ pair in TiO$_2$ [36]. Since the Fermi level energy of TiO$_2$ is higher than that of CuO, the photoexcited e$^-$ from CB of TiO$_2$ moves to the CB of CuO

through rGO layers and hence the $e^- - h^+$ pair recombination is inhibited [56]. This was evident by the PL studies which showed the lowest luminescence intensity for the rGO loaded CuO-TiO$_2$ photocatalyst (Fig. 6). The existence of co-catalyst (CuO) improves the efficiency substantially by preventing the $e^- - h^+$ pair recombination which could be inferred from the results obtained by effect of Cu loading (Fig. S4b in Supplementary Materials). In addition, visible light from the diffused sunlight can excite e^- from the VB of CuO to the CB and as a result h^+ is generated in the VB of CuO. The h^+ present in the VB of both TiO$_2$ and CuO reacts with H$_2$O in the reaction medium and generate •OH radicals and at the same time the e^- is utilized for the conversion of O$_2$ to O_2^-. Furthermore, ultrasound also produces •OH radicals to some extent but the enhancement of catalytic activity in the presence of ultrasound is probably also due to mechanical agitation and mass transfer effects. Synergistic effects obviously supported this observation (Fig. 8). A lower level of degradation was observed with bare TiO$_2$, TiO$_2$/GO and CuO-TiO$_2$ catalysts, whereas CuO-TiO$_2$/rGO photocatalyst showed a profound effect on MO dye degradation. Similarly, the presence of rGO layer enhances the mobility of electron from TiO$_2$ to CuO and hence the catalytic performance is also enhanced, which can be noted from the effect of GO loading (Fig. S4a in Supplementary Materials).

3.13. Effect of benzoic acid and oxygen purging

According to the proposed mechanism discussed above, •OH radicals generated by h^+ and ultrasound are responsible for the degradation of MO. To confirm this, the ultrasound assisted photocatalytic degradation was carried out in presence of a •OH scavenger. Benzoic acid (BA) is commonly used as •OH scavenger in photocatalytic reaction systems to illustrate whether the degradation proceeded by •OH radicals [57]. Hence, the MO degradation was

performed with different BA concentrations (0.25, 0.5 and 1.0 mM). At 0.25 mM of BA, nearly 60% drop in the % degradation efficiency was observed (Fig. S16a in Supplementary Materials). Further increase of BA concentration (0.5 to 1.0 mM) decreased the % degradation to 70 and 77%, respectively (Fig. S16a in Supplementary Materials). This is clear evidence that •OH radicals are mainly responsible for the degradation of the dye under diffused sunlight in the sonophotocatalytic process.

Molecular oxygen (O_2) is commonly used as an electron acceptor to utilize the photo-generated electrons present in CB and form an active superoxide anion (O_2^-). It also prevents the electron-hole pair recombination and hence increases the photocatalytic efficiency [58,59]. O_2 gas was continuously purged to increase the dissolved oxygen content in the reaction medium and there was no major difference observed on the degradation of MO (Fig. S16b in Supplementary Materials) [60,61]. This observation suggests that purging of external O_2 is not necessary for the diffused sunlight driven sonophotocatalytic degradation of MO.

4. Conclusions

A diffused sunlight driven sonophotocatalytic degradation system was developed for the first time using CuO-TiO$_2$/rGO. XRD and XPS analysis confirmed the formation of CuO and anatase-TiO$_2$ by the simple wet impregnation technique. Uniform decoration of CuO-TiO$_2$ nanocomposites over rGO surface was identified by TEM studies. The presence of a co-catalyst (CuO) narrowed down the effective band gap energy of TiO$_2$ as revealed by UV-vis DRS. Moreover, a phenomenal synergistic effect was experienced by combining the ultrasound and photocatalyst for the degradation of MO under diffused sunlight. The solid support, rGO, not only prevented the aggregation of CuO-TiO$_2$ nanocomposites but also increased the carrier mobility and thereby restricted the electron-hole pair recombination as

19

evident by the PL analysis. Sonophotocatalytic degradation pathway was investigated with the aid of LC-MS studies which strongly proved that this sonophotocatalytic system proceeded *via* the degradation of MO using the •OH radicals under diffused sunlight in presence of $CuO-TiO_2/rGO$. Complete degradation of other pollutants such as MB and 4-chlorophenol evident the versatility of this novel sonophotocatalytic degradation process.

Acknowledgments

Appendix A. Supplementary data

Supplementary data associated with this article can be found, in the online version, at http://dx.doi.org/xx.xxxx/j.hazmat.xxxx.xx.xxx.

References

[1] S. Parsons, *Advanced Oxidative Processes for Water and Wastewater Treatment*, IWA Publishing, UK, 2004.

[2] J.C. Colmenares, R. Luque, Heterogeneous photocatalytic nanomaterials: prospects and challenges in selective transformations of biomass-derived compounds, Chem. Soc. Rev. 43 (2014) 765–778.

[3] M.M. Khin, A.S. Nair, V.J. Babu, R. Murugana, S. Ramakrishna, A review on nanomaterials for environmental remediation, Energy Environ. Sci. 5 (2012) 8075–8109.

[4] A. Houas, H. Lachheb, M. Ksibi, E. Elaloui, C. Guillard, J.M. Herrmann, Photocatalytic degradation pathway of methylene blue in water, Appl. Catal. B: Environ. 31 (2001) 145–157.

[5] M.R. Hoffmann, S.T. Martin, W. Choi, D.W. Bahnemann, Environmental Applications of Semiconductor Photocatalysis, Chem. Rev. 95 (1995) 69–96.

[6] K. Konstantinou, T.A. Albanis, TiO_2-assisted photocatalytic degradation of azo dyes in aqueous solution: kinetic and mechanistic investigations: A review, Appl. Catal. B: Environ. 49 (2004) 1–14.

[7] H. Lachheb, E. Puzenat, A. Houas, M. Ksibi, E. Elaloui, C. Guillard, J.M. Herrmann, Photocatalytic degradation of various types of dyes (Alizarin S, Crocein Orange G, Methyl Red, Congo Red, Methylene Blue) in water by UV-irradiated titania, Appl. Catal. B: Environ. 39 (2002) 75–90.

[8] A. D. Bokare, W. Choi, Review of iron-free Fenton-like systems for activating H_2O_2 in advanced oxidation processes, J. Hazard. Mater. 275 (2014) 121–135.

21

[9] G. Zhang, W. Choi, S. H. Kim, S. B. Hong, Selective photocatalytic degradation of aquatic pollutants by titania encapsulated into FAU-type zeolites, J. Hazard. Mater. 188 (2011) 198–205.

[10] S. Ma, J. Xue, Y. Zhou, Z. Zhang, Photochemical synthesis of ZnO/Ag_2O heterostructures with enhanced ultraviolet and visible photocatalytic activity, J. Mater. Chem. A 2 (2014) 7272–7280.

[11] F. Kayaci, S. Vempati, C.O. Akgun, I. Donmez, N. Biyiklia, T. Uyar, Selective isolation of the electron or hole in photocatalysis: $ZnO–TiO_2$ and $TiO_2–ZnO$ core–shell structured heterojunction nanofibers via electrospinning and atomic layer deposition, Nanoscale 6 (2014) 5735–5745.

[12] M. Deo, D. Shinde, A. Yengantiwar, J. Jog, B. Hannoyer, X. Sauvage, M. More, S. Ogale, Cu_2O/ZnO hetero-nanobrush: hierarchical assembly, field emission and photocatalytic properties, J. Mater. Chem. 22 (2012) 17055–17062.

[13] C.C. Chen, C.S. Lu, Y.C. Chung, J.L. Jan, UV light induced photodegradation of malachite green on TiO_2 nanoparticles, J. Hazard. Mater. 141 (2007) 520–528

[14] S.K. Sharma, R. Sanghi, *Advances in Water Treatment and Pollution Prevention, Springer Science*, BMD, 2012.

[15] J.M. Monteagudo, A. Duran, I.S. Martin, S. Garcia, Ultrasound-assisted homogeneous photocatalytic degradation of Reactive Blue 4 in aqueous solution, Appl. Catal. B: Environ. 152–153 (2014) 59–67.

[16] H. Kang, C.S. Lee, D.Y. Kim, J. Kim, W. Choi, H. Kim, Photocatalytic effect of thermal atomic layer deposition of TiO_2 on stainless steel, Appl. Catal. B: Environ. 104 (2011) 6–11.

[17]   K. Vinodgopal, Y. He, M. Ashokkumar, F. Grieser, Sonochemically prepared platinum-ruthenium bimetallic nanoparticles, J. Phys. Chem. B 110 (2006) 3849–3852.

[18]   C. Petrier, Y. Jiang, M.F. Lamy, Ultrasound and environment: sonochemical destruction of chloroaromatic derivatives, Environ. Sci. Technol. 32 (1998) 1316–1318.

[19]   S.P. Meshram, D.T. Tayade, P.D. Ingle, P.D. Jolhe, B.B. Diwate, S.B. Biswas, Ultrasonic cavitation induced degradation of Congo red in aqueous solutions, Chem. Eng. Res. Bull. 14 (2010) 119–123.

[20]   L. Weavers, N. Malmstadt, M.R. Hoffmann, Kinetics and mechanism of pentachlorophenol degradation by sonication, ozonation, and sonolytic ozonation, Environ. Sci. Technol. 34 (2000) 1280–1285.

[21]   B. Neppolian, H. Jung, H. Choia, J.H. Leea, J.W. Kang, Sonolytic degradation of methyl *tert*-butyl ether: the role of coupled Fenton process and persulphate ion, Water Res. 36 (2002) 4699–4708.

[22]   D.D. Dionysioua, M.T. Suidana, E. Bekoua, I. Baudin, J.M. Laine, Effect of ionic strength and hydrogen peroxide on the photocatalytic degradation of 4-chlorobenzoic acid in water, Appl. Catal. B: Environ. 26 (2000) 153–171.

[23]   R. Singla, F. Grieser, M. Ashokkumar, Sonochemical degradation of martius yellow dye in aqueous solution, Ultrason. Sonochem. 16 (2009) 28–34.

[24]   B. Neppolian, A. Doronila, M. Ashokkumar, Sonochemical oxidation of arsenic(III) to arsenic(V) using potassium peroxydisulfate as an oxidizing agent, Water. Res. 44 (2010) 3687–3695.

[25] C. Comninellis, A. Kapalka, S. Malato, S.A. Parsons, I. Poulios, D. Mantzavinos, Advanced oxidation processes for water treatment: advances and trends for R&D, J. Chem. Technol. Biotechnol. 83 (2008) 769–776.

[26] M. Mrowetz, C. Pirola, E. Selli, Degradation of organic water pollutants through sonophotocatalysis in the presence of TiO_2, Ultrason. Sonochem. 10 (2003) 247–254.

[27] E. Selli, Synergistic effects of sonolysis combined with photocatalysis in the degradation of an azo dye, Phys. Chem. Chem. Phys. 4 (2002) 6123–6128.

[28] D.E. Kritikos, N.P. Xekoukoulotakis, E. Psillakis, D. Mantzavinos, Photocatalytic degradation of reactive black 5 in aqueous solutions: Effect of operating conditions and coupling with ultrasound irradiation, Water Res. 41 (2007) 2236–2246.

[29] B. Neppolian, L. Ciceri, C. L. Bianchi, F. Grieser, M. Ashokkumar, Sonophotocatalytic degradation of 4-chlorophenol using $Bi_2O_3/TiZrO_4$ as a visible light responsive photocatalyst, Ultrason. Sonochem. 18 (2011) 135–139.

[30] G.K. Parshetti, A.A. Telke, D.C. Kalyani, S.P. Govindwar, Decolorization and detoxification of sulfonated azo dye methyl orange by Kocuria rosea MTCC 1532, J. Hazard. Mater. 176 (2010) 503–509.

[31] N. Mathur, P. Bhatnagar, P. Sharma, Review of the mutagenicity of textile dye products, Univ. J. Environ. Res. Tech. 2 (2012) 1–18.

[32] J.P. Brown, P.S. Dietrich, Mutagenicity of selected sulfonated azo dyes in the Salmonella/microsome assay: Use of aerobic and anaerobic activation procedures, Mutat. Res. 116 (1983) 305–315.

[33] W.S. Hummers, R.E. Offeman, Preparation of graphitic oxide, J. Am. Chem. Soc. 80 (1958) 1339.

[34] J.C. Yu, L. Zhang, J. Yu, Rapid synthesis of mesoporous TiO_2 with high photocatalytic activity by ultrasound-induced agglomeration, New J. Chem. 26 (2002) 416–420.

[35] J.H. Pana, X.S. Zhaoa, W.I. Lee, Block copolymer-templated synthesis of highly organized mesoporous TiO_2-based films and their photoelectrochemical applications, Chem. Eng. J. 170 (2011) 363–380.

[36] D.P. Kumar, M.V. Shankar, M.M. Kumari, G. Sadanandam, B. Srinivas, V. Durgakumari, Nano-size effects on CuO/TiO_2 catalysts for highly efficient H_2 production under solar light irradiation, Chem. Commun. 49 (2013) 9443–9445.

[37] Y.C. Lee, Y.S. Chang, L.G. Teoh, Y.L. Huang, Y.C. Shen, The effects of the nanostructure of mesoporous TiO_2 on optical band gap energy, J. Sol-Gel Sci. Techol. 56 (2010) 33–38.

[38] S.G. Babu, R. Karvembu, CuO Nanoparticles: A simple, effective, ligand free and reusable heterogeneous catalyst for N-arylation of benzimidazole, Ind. Eng. Chem. Res. 50 (2011) 9594–9600.

[39] S.G. Babu, R. Karvembu, Room temperature Ullmann type C–O and C–S cross coupling of aryl halides with phenol/thiophenol catalyzed by CuO nanoparticles, Tetrahedron Lett. 54 (2013) 1677–1680.

[40] M. Gopiraman, S.G. Babu, Z. Khatri, K. Wei, Y.A. Kim, M. Endo, R. Karvembu, I.S. Kim, Dry Synthesis of Easily Tunable Nano Ruthenium Supported on Graphene:

Novel Nanocatalysts for Aerial Oxidation of Alcohols and Transfer Hydrogenation of Ketones, J. Phys. Chem. C. 117 (2013) 23582−23596.

[41]   B. Chai, T. Peng, X. Zhang, J. Mao, K. Li, X. Zhang, Synthesis of C_{60}-decorated SWCNTs (C_{60}-d-CNTs) and its TiO_2-based nanocomposite with enhanced photocatalytic activity for hydrogen production, Dalton Trans. 42 (2013) 3402–3409.

[42]   M. Gopiraman, S.G. Babu, Z. Khatri, K. Wei, M. Endo, R. Karvembu, I. S. Kim, Facile and homogeneous decoration of RuO_2 nanorods on graphene nanoplatelets for transfer hydrogenation of carbonyl compounds, Catal. Sci. Technol. 3 (2013) 1485–1489.

[43]   K. Vinodgopal, B. Neppolian, I.V. Lightcap, F. Grieser, M. Ashokkumar, P.V. Kamat, Sonolytic design of graphene-Au nanocomposites. Simultaneous and sequential reduction of graphene oxide and Au(III), J. Phys. Chem. Lett. 1 (2010) 1987–1993.

[44]   S. Pei, H.M. Cheng, The reduction of graphene oxide, Carbon 50 (2012) 3210–3228.

[45]   S.G. Babu, N. Neelakandeswari, N. Dharmaraj, S.D. Jackson, R. Karvembu, Copper(II) oxide on aluminosilicate mediated Heck coupling of styrene with aryl halides in water, RSC Adv. 3 (2013) 7774−7781.

[46]   M. Gopiraman, S.G. Babu, Z. Khatri, K. Wei, Y.A. Kim, M. Endo, R. Karvembu, I.S. Kim, An efficient, reusable copper-oxide/carbon-nanotube catalyst for N-arylation of imidazole, Carbon 62 (2013) 135–148.

[47]   G. M. An, W.H. Ma, Z.Y. Sun, Z.M. Liu, B.X. Han, S.D. Miao, Z.J. Miao, K.L. Ding, Preparation of titania/carbon nanotube composites using supercritical ethanol and

their photocatalytic activity for phenol degradation under visible light irradiation, Carbon 45 (2007) 1795–1801.

[48]   B. Srinivas, K. Lalitha, P.A.K. Reddy, G. Rajesh, V.D. Kumari, M. Subrahmanyam, B.R. De, Cyclohexanol dehydrogenation over Cu-loaded TiO_2 photocatalyst under solar illumination, Res. Chem. Intermed. 37 (2011) 1069–1086.

[49]   K. Lalitha, J.K. Reddy, M.V.P. Sharma, V.D. Kumari, M. Subrahmanyam, Continuous hydrogen production activity over finely dispersed Ag_2O/TiO_2 catalysts from methanol:water mixtures under solar irradiation: A structure–activity correlation, Int. J. Hydrogen Energy 35 (2010) 3991–4001.

[50]   M.Q. Yang, N. Zhang, M. Pagliaro, Y.J. Xu, Artificial photosynthesis over graphene–semiconductor composites. Are we getting better?, Chem. Soc. Rev. 43 (2014) 8240–8254.

[51]   D.C. Hurum, A.G. Agrios, K.A. Gray, T. Rajh, M.C. Thurnauer, Explaining the Enhanced Photocatalytic Activity of Degussa P25 Mixed-Phase TiO_2 Using EPR, J. Phys. Chem. B 107 (2003) 4545–4549.

[52]   S. Hu, A. Wang, X. Li,Y. Wang, H. Lowe, Hydrothermal Synthesis of Ionic Liquid [Bmim]OH-Modified TiO_2 Nanoparticles with Enhanced Photocatalytic Activity under Visible Light, Chem. Asian J. 5 (2010) 1171–1177.

[53]   B. Neppolian, A. Bruno, C.L. Bianchi, M. Ashokkumar, Graphene oxide based Pt–TiO_2 photocatalyst: Ultrasound assisted synthesis, characterization and catalytic efficiency, Ultrason. Sonochem. 19 (2012) 9–15.

27

[54] J. Zhang, Z. Xionga, X.S. Zhao, Graphene–metal–oxide composites for the degradation of dyes under visible light irradiation, J. Mater. Chem. 21 (2011) 3634–3640.

[55] Y. He, F. Grieser, M. Ashokkumar, The mechanism of sonophotocatalytic degradation of methyl orange and its products in aqueous solutions, Ultrason. Sonochem. 18 (2011) 974–980.

[56] J. Bandara, C.P.K. Udawatta, C.S.K. Rajapakse, Highly stable CuO incorporated TiO_2 catalyst for photocatalytic hydrogen production from H_2O, Photochem. Photobiol. Sci. 4 (2005) 857–861.

[57] P.K. Dutta, S.O. Pehkonen, V.K. Sharma, A.K. Ray, Photocatalytic Oxidation of Arsenic(III): Evidence of Hydroxyl Radicals, Environ. Sci. Technol. 39 (2005) 1827–1834.

[58] S. Zhu, X. Yang, W. Yang, L. Zhang, J. Wang, M. Huo, Application of Porous Nickel-Coated TiO_2 for the Photocatalytic Degradation of Aqueous Quinoline in an Internal Airlift Loop Reactor, Int. J. Environ. Res. Public Health 9 (2012) 548–563.

[59] C.H. Hung, B.J. Marinas, Role of chlorine and oxygen in the photocatalytic degradation of trichloroethylene vapor on TiO_2 films, Environ. Sci. Technol. 31 (1997) 562–568.

[60] J.N. Brown, M. Hewins, J.H.M. Van der linden, R.J. Lynch, Solvent degassing and other factors affecting liquid chromatographic detector stability, J. Chromarogr. A 204 (1981) 115–l 22.

[61] M.E. Rollie, G. Patonay, I.M. Warner, Deoxygenation of solutions and its analytical applications, Ind. Eng. Chem. Res. 26 (1987) 1–6.

28
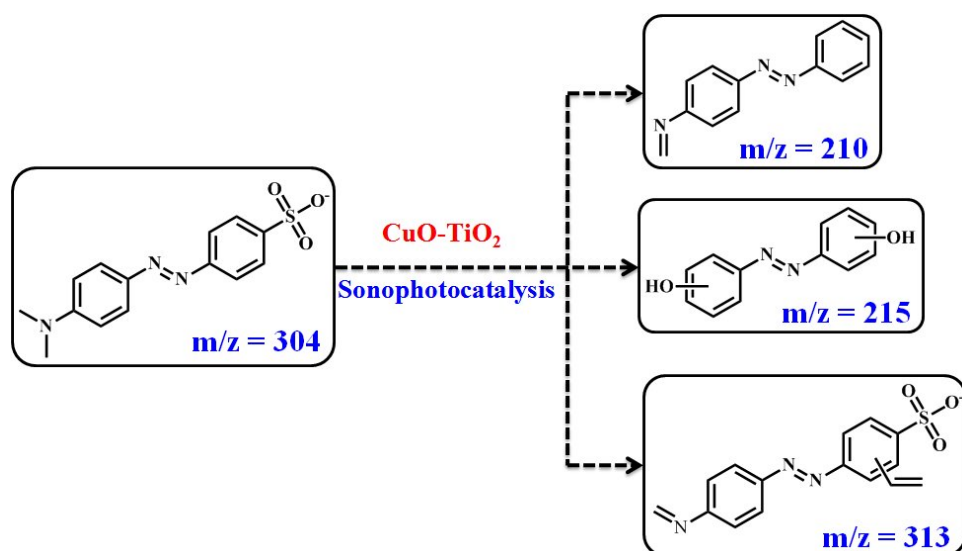
Scheme 1. Structure of by-products formed from MO during the sonophotocatalytic degradation using CuO-TiO₂ photocatalyst.
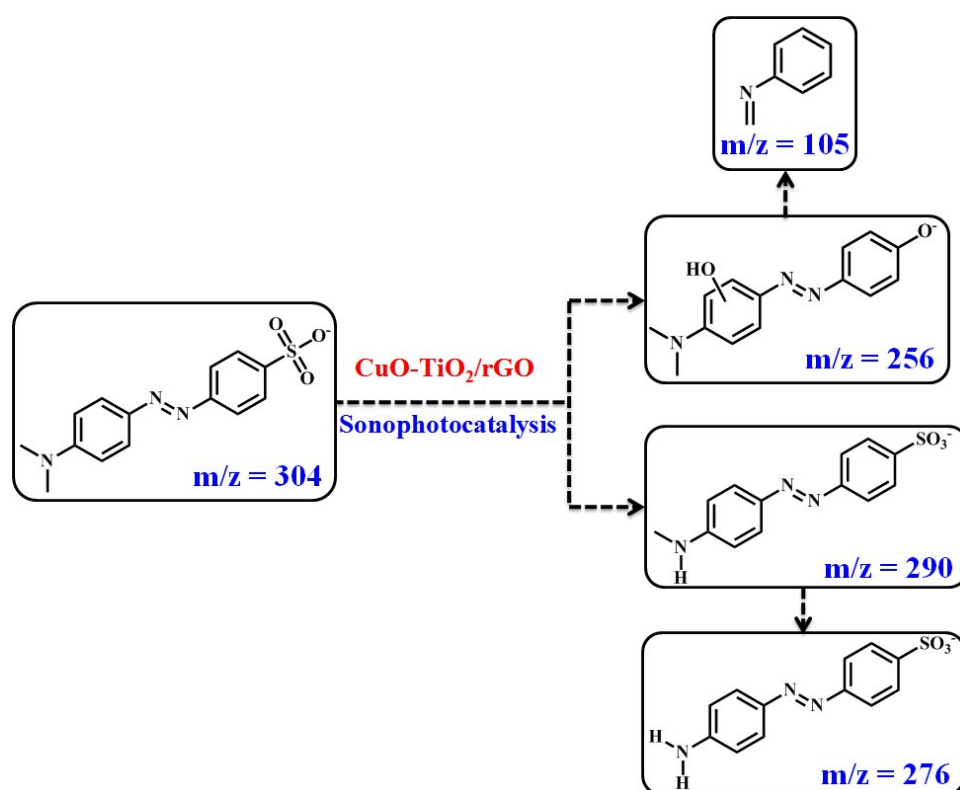
Scheme 2. Structure of by-products formed from MO during the sonophotocatalytic degradation using CuO-TiO₂/rGO photocatalyst.
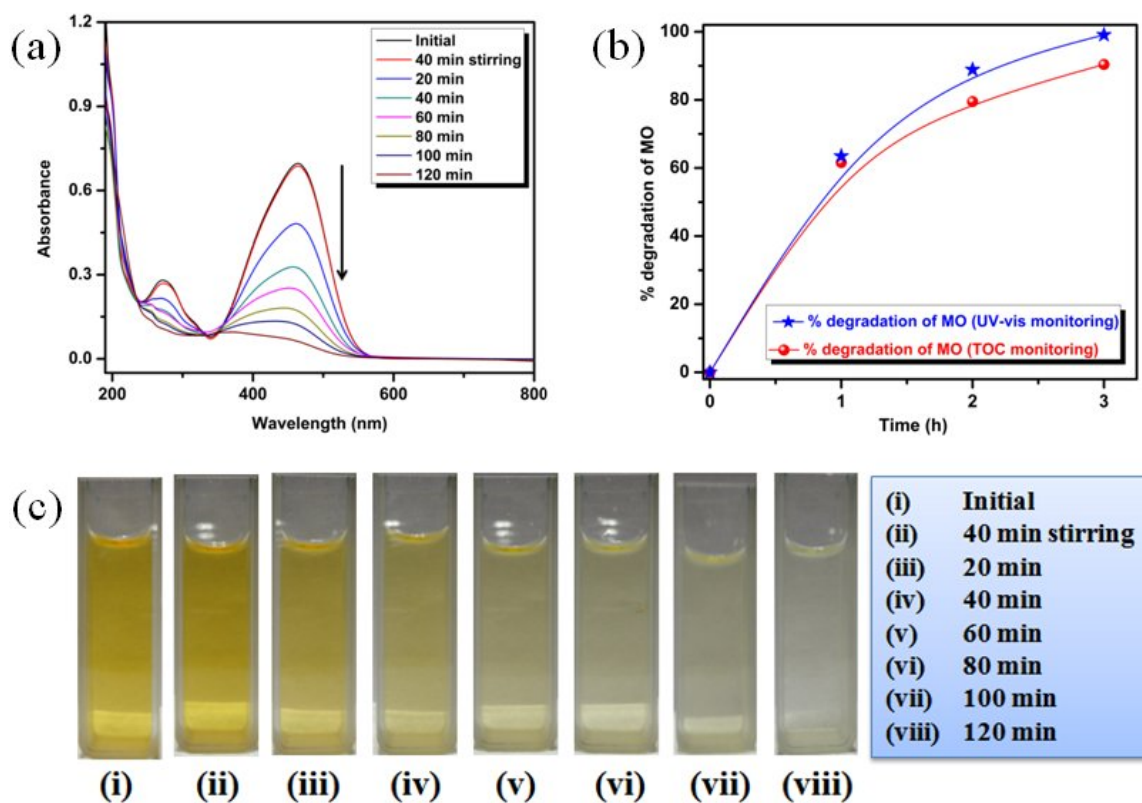
Fig. 1. (a) UV-vis spectra, (b) TOC monitoring and (b) photographic evidence of degradation of methyl orange (MO) at various time intervals.
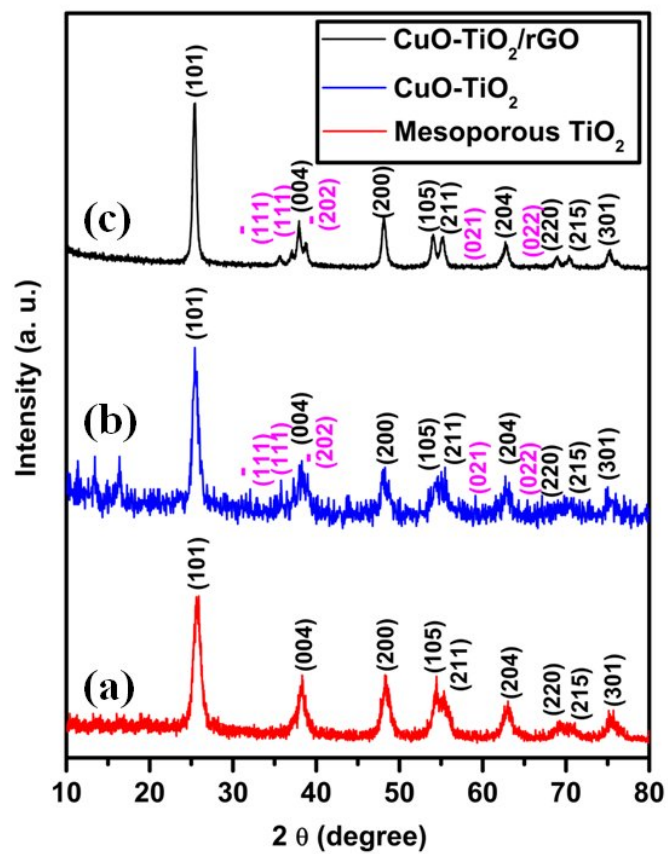
Fig. 2. XRD patterns of (a) mesoporous TiO_2 NPs, (b) $CuO-TiO_2$ and (c) $CuO-TiO_2/rGO$.
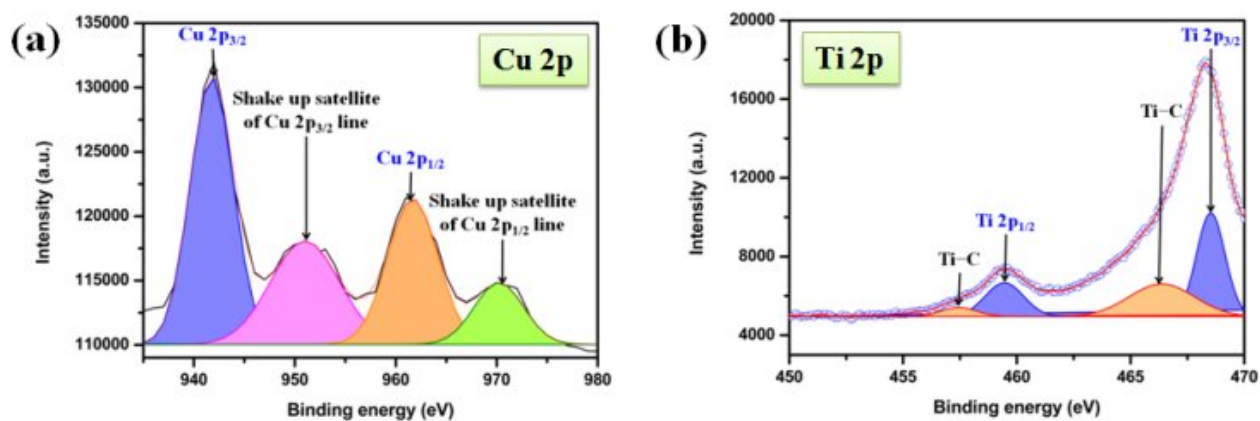
Fig. 3. XPS spectra of the CuO-TiO$_2$/rGO: (a) high resolution Cu 2p spectrum and (b) high resolution Ti 2p spectrum.
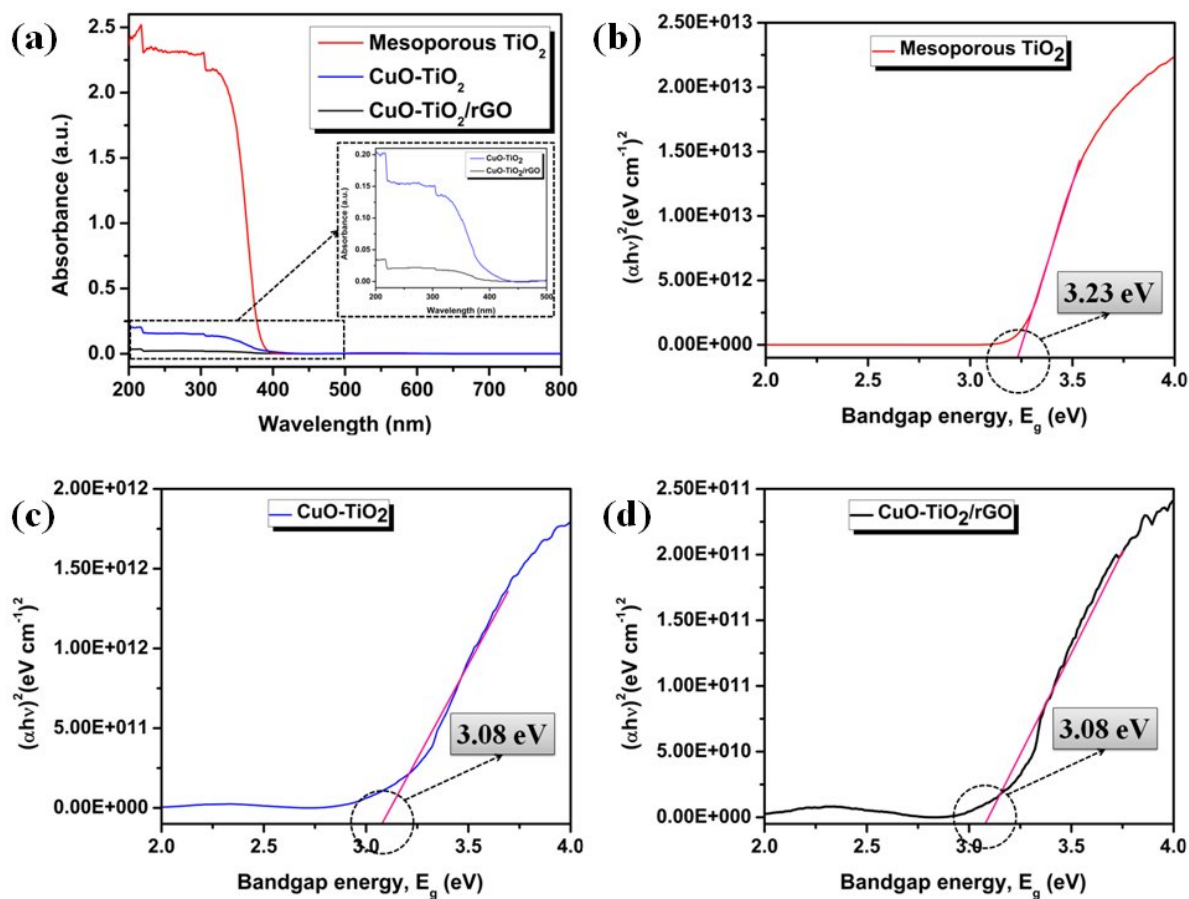
Fig. 4. (a) UV-vis absorption spectra (DRS mode) of mesoporous TiO$_2$ NPs, CuO-TiO$_2$ and CuO-TiO$_2$/rGO and Tauc plot of (b) TiO$_2$ (c) CuO-TiO$_2$ and (d) CuO-TiO$_2$/rGO.
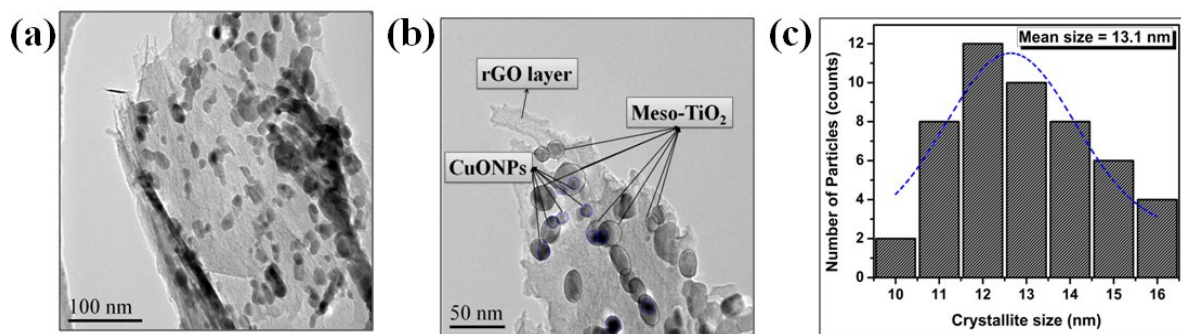
Fig. 5. TEM images of CuO-TiO$_2$/rGO nanocatalyst (a) 100 nm, (b) 50 nm, and the corresponding (c) crystallite size distribution graph.
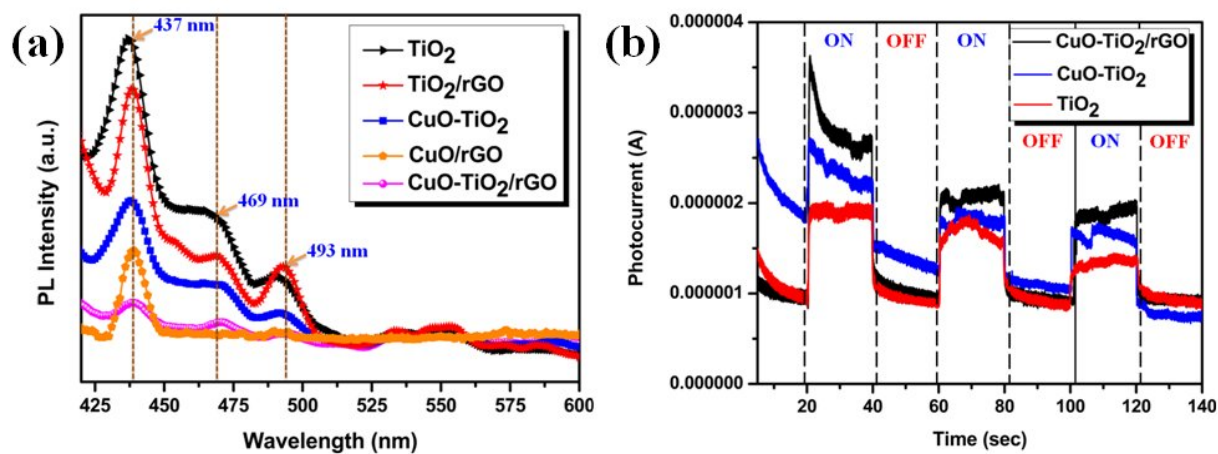
Fig. 6. (a) Photoluminescence spectra of TiO_2, TiO_2/rGO, CuO-TiO_2, CuO/rGO and CuO-TiO_2/rGO, and (b) photoelectrochemical studies of TiO_2, CuO-TiO_2 and CuO-TiO_2/rGO.
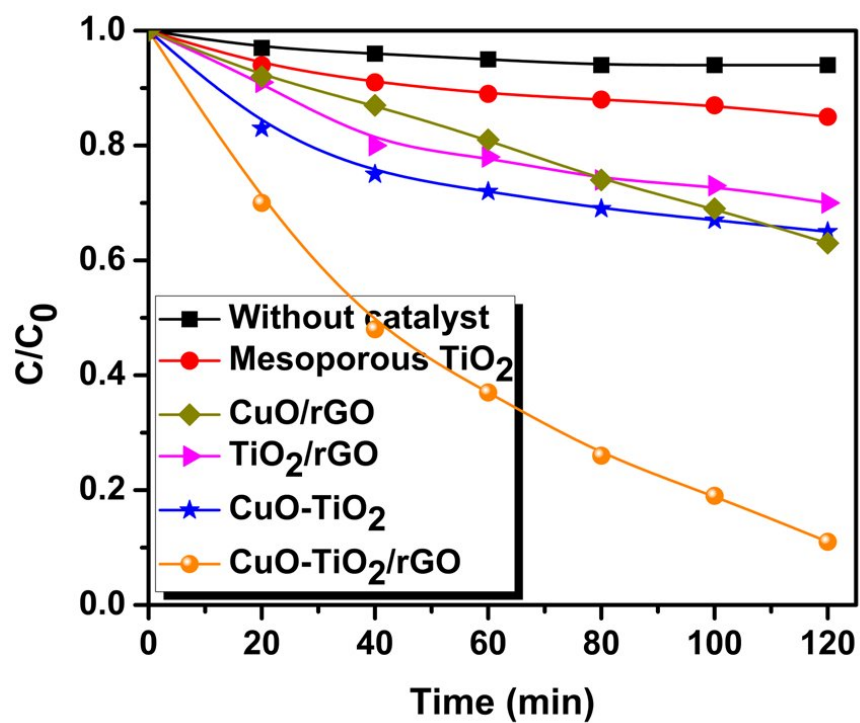
Fig. 7. Sonophotocatalytic degradation of MO under diffused sunlight with different photocatalysts.
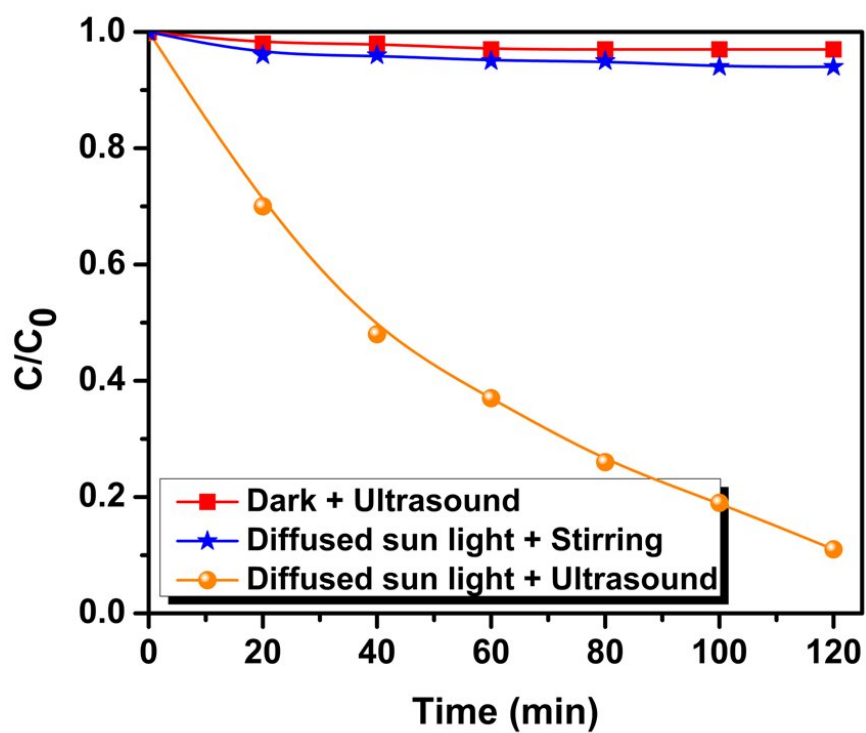
Fig. 8. Synergistic effect of ultrasound on photocatalytic degradation of MO under diffused sunlight.

38
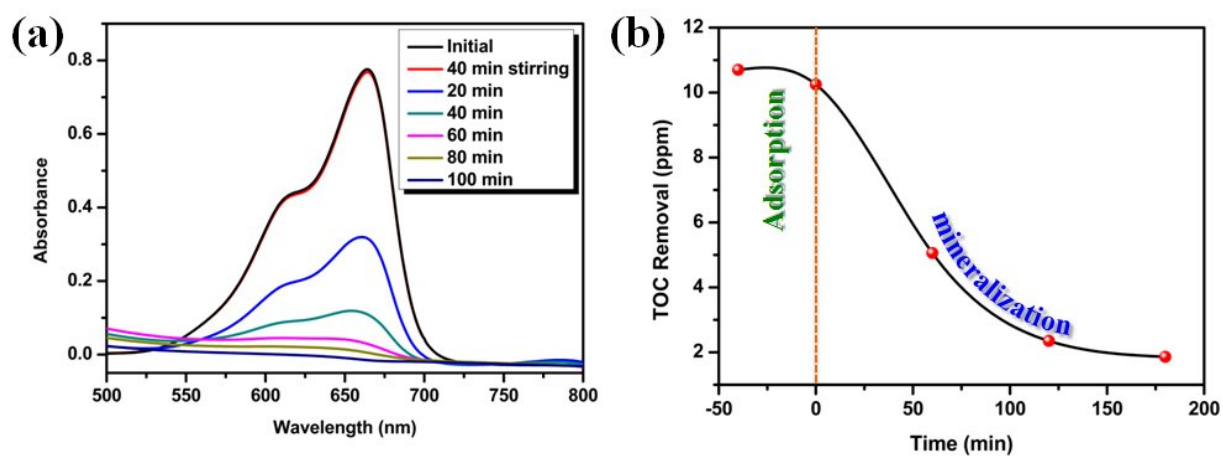
Fig. 9. Sonophotocatalytic degradation of (a) methylene blue and (b) 4-chlorophenol using CuO-TiO$_2$/rGO under diffused sunlight.
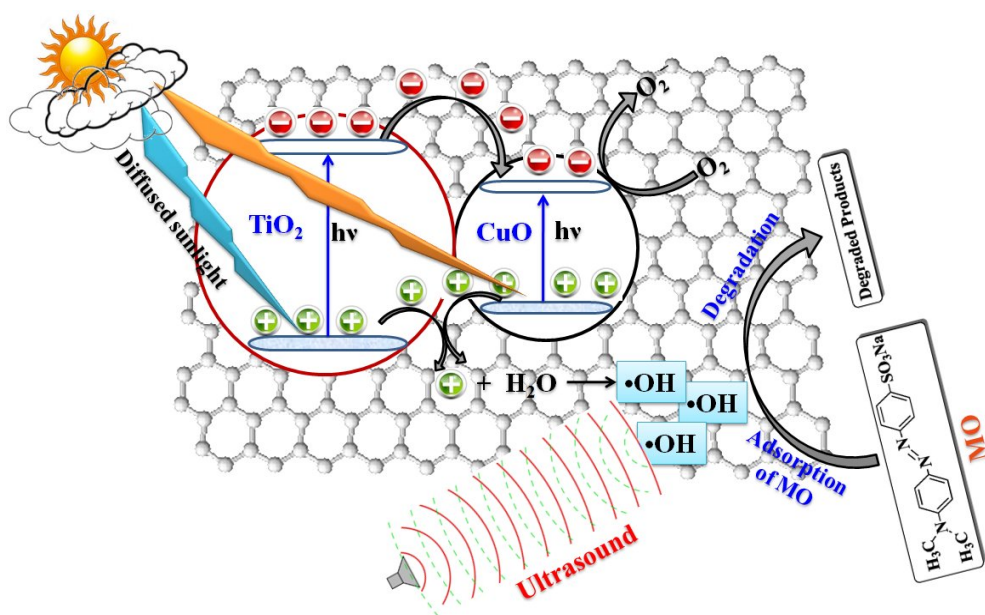
Fig. 10. Plausible mechanism for the ultrasound assisted photocatalytic degradation of MO under diffused sunlight.

Diffused sunlight driven highly synergistic pathway for complete mineralization of organic contaminants using reduced graphene oxide supported photocatalyst

Sundaram Ganesh Babu[a], RamalingamVinoth[a], Bernaurdshaw Neppolian[a,*], Dionysios D. Dionysiou[b], Muthupandian Ashokkumar[c]

[a] *SRM Research Institute, SRM University, Kattankulathur 603203, Chennai, Tamilnadu, India*
[b] *Environmental Engineering and Science Program, Department of Biomedical, Chemical and Environmental Engineering, University of Cincinnati, Cincinnati, OH 45221-0012, USA*
[c] *The School of Chemistry, University of Melbourne, Parkville, Melbourne, Victoria 3010, Australia*

Supplementary Materials

Materials and methods

Graphite powder (synthetic, conducting grade, 325 mesh, 99.9995%) was obtained from Alfa Aesar. $Cu(NO_3)_2 \cdot 3H_2O$ was procured from Loba Chemie Pvt. Ltd. $NaNO_3$, $KMnO_4$ and H_2SO_4 were purchased from Rankem, India. MO was purchased from Sigma Aldrich. Milli-Q ultrapure water through Q-POD (Merck Millipore system, conductivity 18.2 $M\Omega$) was used in all experiments.

An ultrasonic bath (WENSAR, 40 kHz and 25 L capacity, India) was used for the sonophotocatalytic degradation of MO. An ultrasonic horn operating at 20 kHz (SONICS, Vibra cell, USA) was used for the synthesis of photocatalyst. Unless otherwise noted all reactions were carried out at 30±3 ºC. Sonophotocatalytic degradation reactions were performed in the Energy and Environmental Remediation Lab, 13th Floor of SRM University main building under diffused sun light with 1000-1300 LUX intensity.

Characterization studies of the prepared photocatalysts

In order to understand the crystal structure of $CuO-TiO_2/rGO$ photocatalyst, X-ray diffraction (XRD) studies were carried out using PANaltical X'pert powder diffractometer using Cu Kα radiation. UV-vis DRS measurements were carried out over Shimadzu UV-2600 UV-vis spectrophotometer in DRS mode. The surface morphology and weight percentage of Cu and Ti in $CuO-TiO_2/rGO$ photocatalyst were determined by SEM-EDS analysis (FEI Quanta FEG 200 HR-SEM) which operated at 20 kV. The particle size and size distribution of $CuO-TiO_2$ over rGO layer were investigated using TEM (JEM-2100 JEOL Japan) with accelerating voltage of 120 kV. Image J software was used to determine the size distribution of particles. X-ray photoelectron spectroscopic (XPS) data were recorded using a Kratos Axis-Ultra DLD spectrometer with Mg-Kα radiation. Photoluminescence (PL) spectra were recorded on a Jasco FP-8300

2

spectrophotometer in the wavelength range, 420–600 nm using an excitation wavelength of 380 nm.

Photoelectrochemical studies

CHI608E electrochemical workstation was used on a in a conventional three electrode configuration with a Pt-wire as counter electrode and Ag/AgCl (in saturated KCl) as a reference electrode to carry out the photoelectrochemical measurements. A light source of 250 W Xe arc lamp (OSRAM, Germany) was used for photocurrent measurements. A 0.1 M Na_2SO_4 aqueous solution was used as the electrolyte. The working electrode was prepared by mixing the 50 mg of photocatalyst with 150 mL of PEG (mol. wt 400) and 125 mL of ethanol was used to make slurry. Then it was coated on a 2.5×2.5 cm^2 fluorine-doped tin oxide (FTO) glass substrate with an active area of about 1×1 cm^2 by doctor-blade method using scotch tape as spacer. It was dried in air and then annealed at 350 ºC for 45 min.

HPLC analysis

HPLC analysis was carried out using Agilent Technologies 1200 series chromatograph with 1260 UV-vis diode array detector. Shim pack VP-ODS column (150 mm L X 2.0 mm ID, 5 µm particle size) from Shimadzu, Japan was used. 20 µL of sample was injected with the flow rate of 200 µL min^{-1} and acetonitrile (30%) and 0.01 M aqueous ammonium acetate (70%) was used as mobile phase. Mass spectra were recorded over an Agilent HPLC coupled with Shimadzu LC-MS 2020 mass spectrometer (Shimadzu, Japan). Electrospray ionization source was operated at negative polarity which was scanned in the range 100-400 *m/z* at the interface temperature 350 ºC.
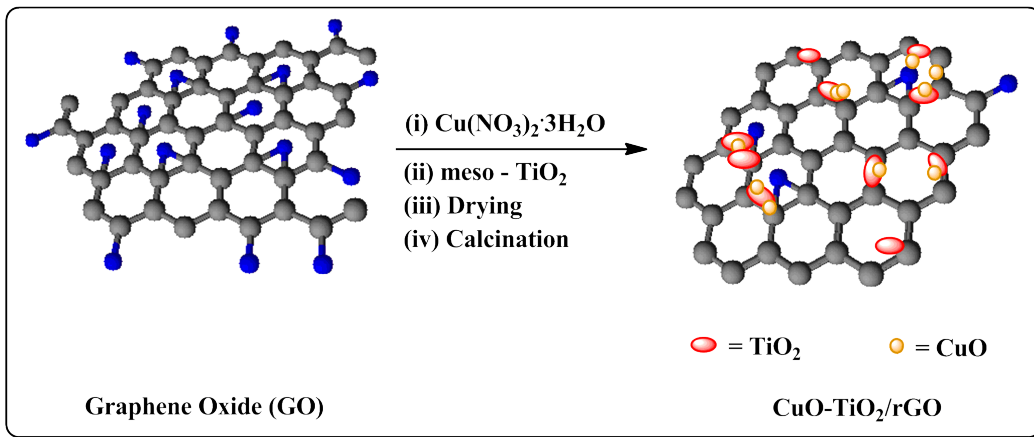
Fig. S1 Preparation of CuO-TiO$_2$/rGO nanocatalyst.

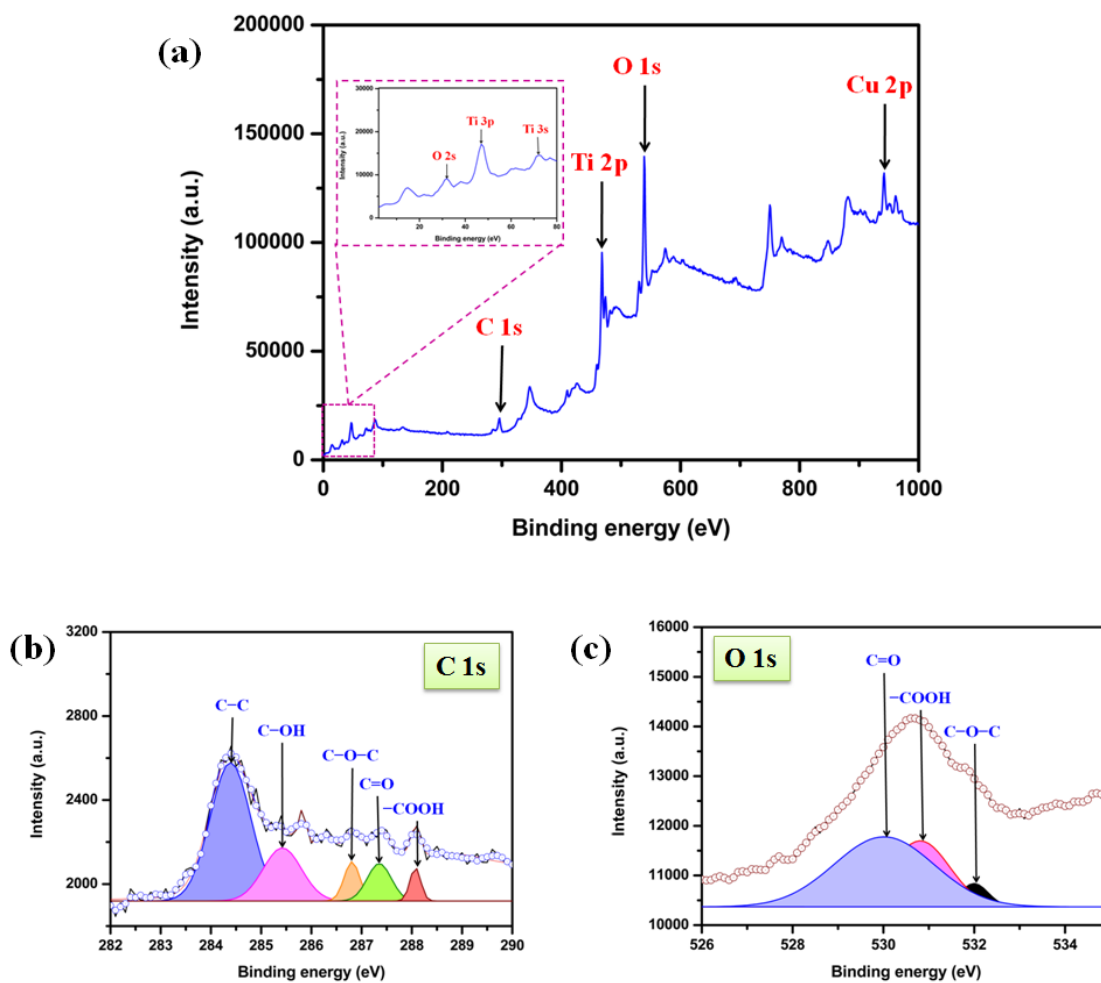**Fig. S2** XPS spectra of the CuO-TiO$_2$/rGO: (a) XPS survey spectrum [inset: magnified view of

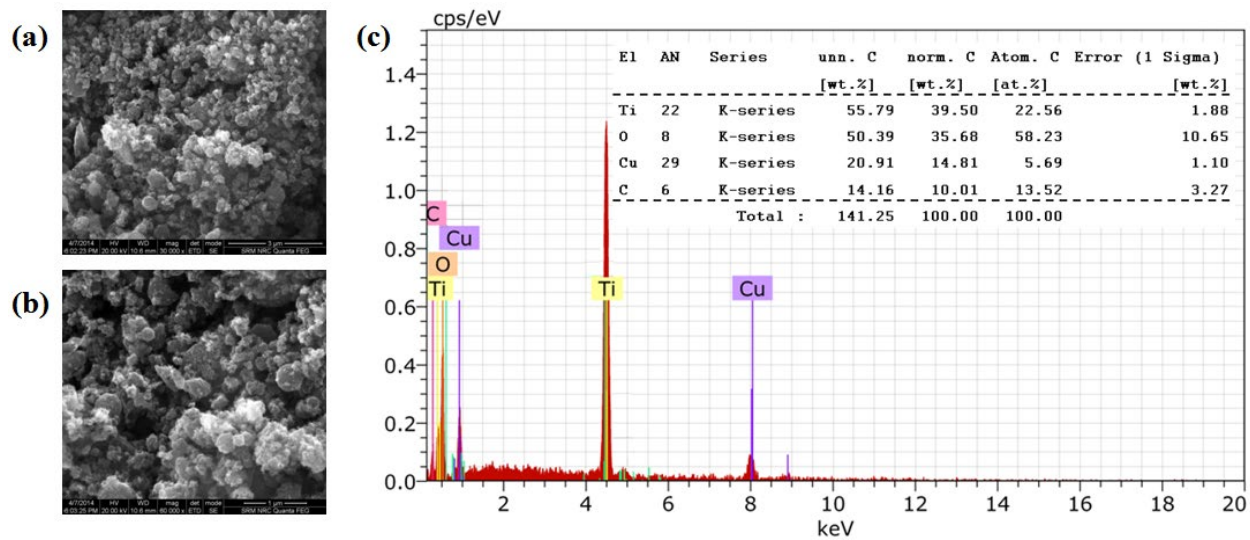0-80 eV region], (b) high resolution C 1s spectrum and (c) high resolution O 1s spectrum.

Fig. S3 SEM images of CuO-TiO$_2$/rGO nanocatalyst with different magnifications (a) scale bar is 3 μm and (b) scale bar is 1 μm and, the corresponding (c) EDS spectrum [inset: weight percentage table].
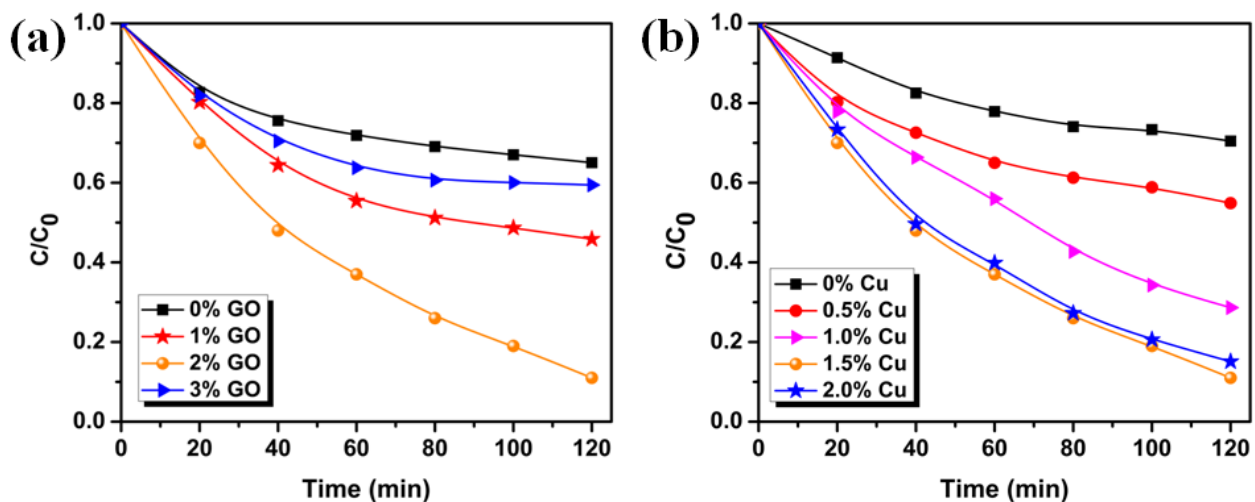

Fig. S4 Effect of (a) GO loading and (b) Cu loading in ultrasound assisted photocatalytic degradation of MO under diffused sun light.

Synergistic effect for the degradation of MO in ultrasonic irradiation under diffused sunlight was calculated as per the following equation (S1-S3) and the value found was 9.98 fold (S4).

$$\text{Synergistic effect} = \frac{[\% \text{ Deg.}]_{US+\text{Diffused Sunlight}}}{[\% \text{ Deg.}]_{US} + [\% \text{ Deg.}]_{\text{Diffused Sunlight}}} \quad \dots\dots\dots\dots\dots\dots\dots\dots\dots\dots\dots\dots\text{(S1)}$$

$$= \frac{88.9}{3.2+5.7} \quad \dots\dots\dots\dots\dots\dots\dots\dots\dots\dots\dots\dots\text{(S2)}$$

$$= \frac{88.9}{8.9} \quad \dots\dots\dots\dots\dots\dots\dots\dots\dots\dots\dots\dots\text{(S3)}$$

$$= 9.98 \quad \dots\dots\dots\dots\dots\dots\dots\dots\dots\dots\dots\dots\text{(S4)}$$

Effects of catalyst dosage and dye concentration

It is important to study the effects of both the amount of catalyst and the concentration of the dye on the rate of degradation of MO under the experimental conditions used in this study. In order to obtain the optimum catalyst dosage, a series of experiments were carried out by varying the catalyst amount, *viz,* 50, 75, 100 and 125 mg per 100 mL of MO and the corresponding extents of degradation observed were 18, 57, 89 and 49%, respectively (Fig. S5a in Supplementary Materials). Based on these results a maximum efficiency was observed with 100 mg of catalyst. This can be explained by the fact that while increasing the catalyst concentration, the active sites of the photocatalyst is increased, subsequently enhancing the •OH radical formation [1]. Further increase in the catalyst amount decreased the photocatalytic degradation efficiency which might be attributed to the screening effect of light by the excess amount of photocatalyst particles in the solution as reported elsewhere [2,3].

Likewise, the effect of dye concentration was also examined for different initial concentrated MO solution (0.01, 0.02, 0.03 and 0.04 mM) with optimized catalyst amount (1.0 g

L^{-1}). Alike in many previous reports, rate of degradation was varied with the initial concentration of MO (Fig. S5b in Supplementary Materials) [4]. As the initial concentration of MO increases from 0.01, 0.02, 0.03 and 0.04 mM, the apparent rate constant decreases gradually to 0.0706, 0.0479, 0.0240 and 0.0151 min^{-1}, respectively (Table S1, entries 1-4 in Supplementary Materials). In other words, the complete degradation of the MO solution with lower concentration (0.01 mM) was attained at lower reaction time (60 min). Whereas the 100% degradation of high concentrated MO solution (0.04 mM) was achieved only after prolonged ultrasonication under diffused sunlight (280 min). This might be attributed to the fact that the high dye concentration may lead to the adsorption of more dye molecules on the surface of CuO-TiO$_2$/rGO photocatalyst. Existence of such large amounts of adsorbed dye molecules on the catalyst's surface results in lack of direct contact between the holes (h$^+$) and H$_2$O to produce •OH radicals and thereby inhibiting the dye degradation. Nevertheless it is noteworthy to mention here that this diffused sunlight driven sonophotocatalytic degradation protocol can be applied for a wide range of initial concentrated organic contaminants.
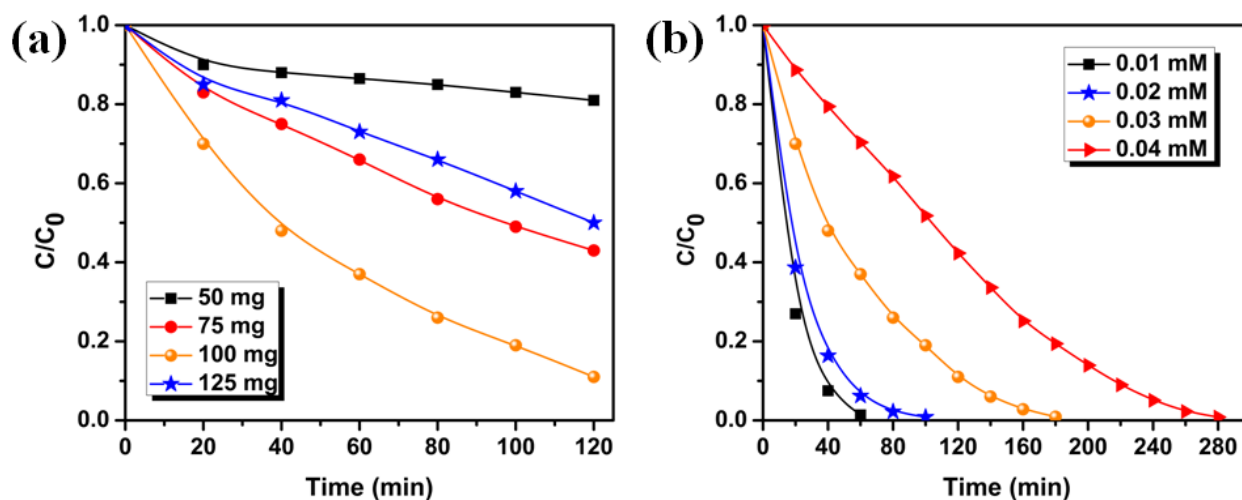
Fig. S5 (a) Optimization of catalyst loading and (b) effect of initial concentration of MO.

Table S1. Effect of initial MO concentration on sonophotocatalytic degradation under diffused sunlight

Entry	Initial concentration of MO (mM)	k' (min⁻¹)	R^2
1	0.01	0.0706	0.99314
2	0.02	0.0479	0.99905
3	0.03	0.02402	0.94308
4	0.04	0.01513	0.87855

Heterogeneity test

In order to test the leaching of active species (CuO-TiO$_2$) from the solid support (rGO) during the course of the reaction, heterogeneity test was carried out (Fig. S6). In brief, two degradation reactions were performed simultaneously under identical experimental conditions in presence of CuO-TiO$_2$/rGO photocatalyst and the progress of the reaction was monitored with UV-vis spectrophotometer. After 60 min of reaction time, the photocatalyst was removed from one of the reaction media by centrifugation (10000 rpm for 10 min) and then allowed to proceed further under sonophotocatalytic degradation with diffused sunlight. It was found that there was a gradual increase of % degradation of MO as usual in the presence of catalyst but there was no further degradation of MO occurred after the removal of photocatalyst in the second system. This set of reactions reveals not only the heterogeneous nature of the photocatalyst but also confirmed that there was no leaching of active species (CuO-TiO$_2$) from the solid support (rGO) during the course of the reaction, i.e. the stability of the catalyst under the sonochemical reaction. Furthermore, these

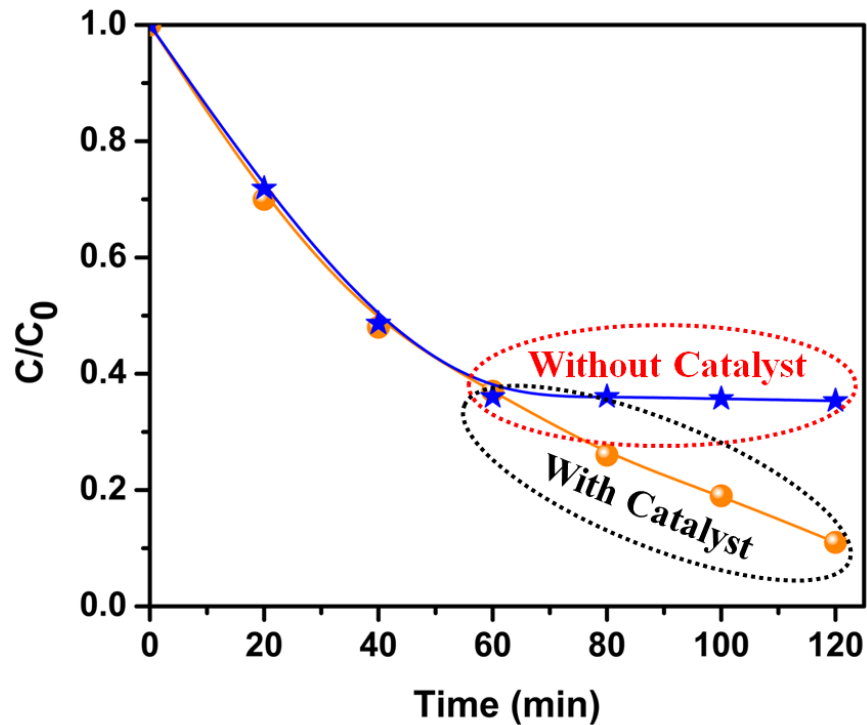results suggested that the MO degradation proceeded only in the presence of catalyst.
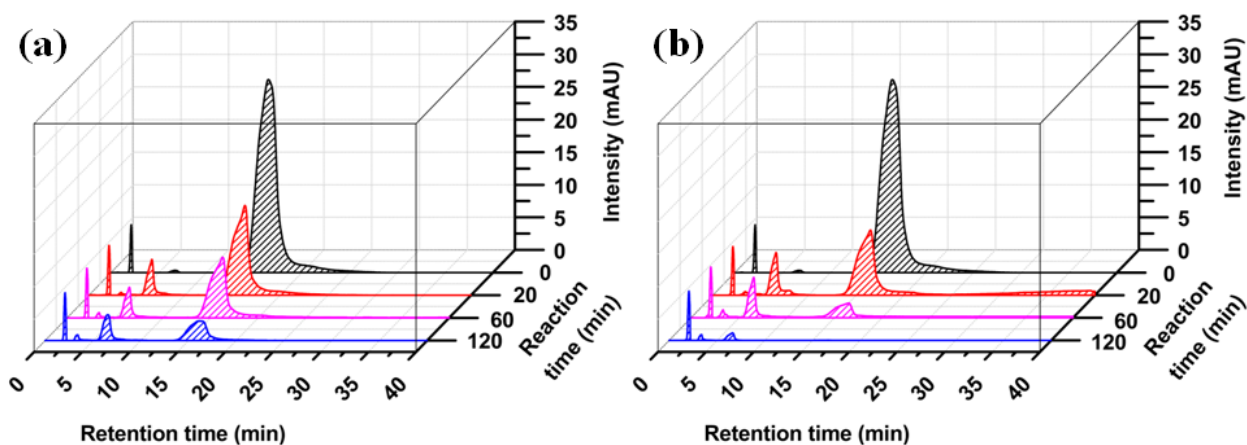

Fig. S6 Heterogeneity tests.

Fig. S7 HPLC chromatograms of MO at different time intervals of sonophotocatalytic degradation using (a) CuO-TiO$_2$ and (b) CuO-TiO$_2$/rGO.
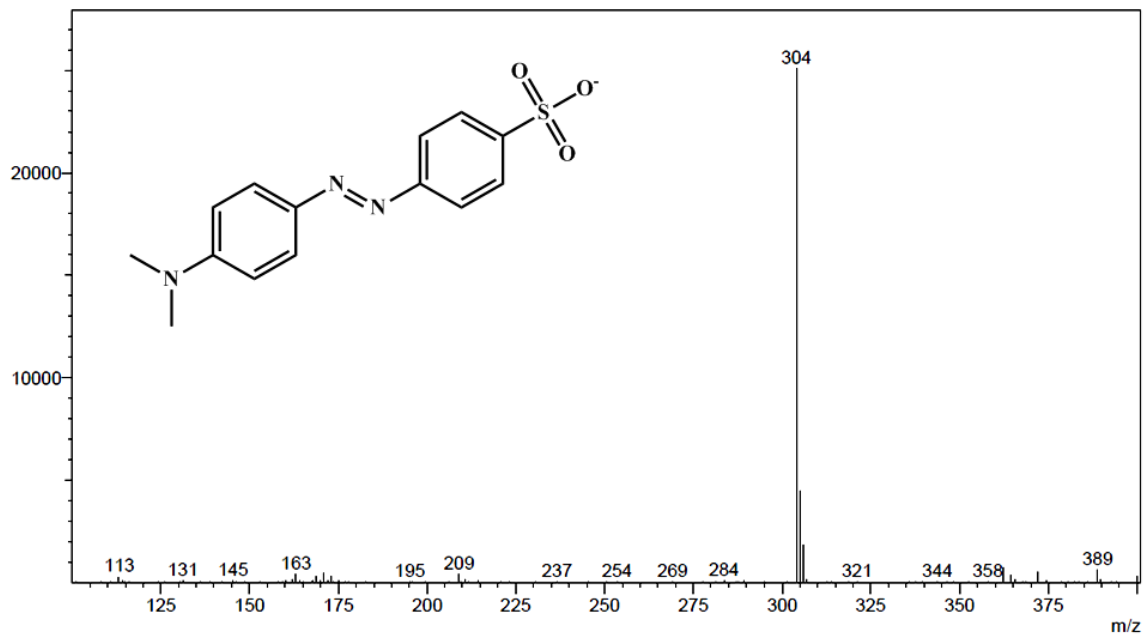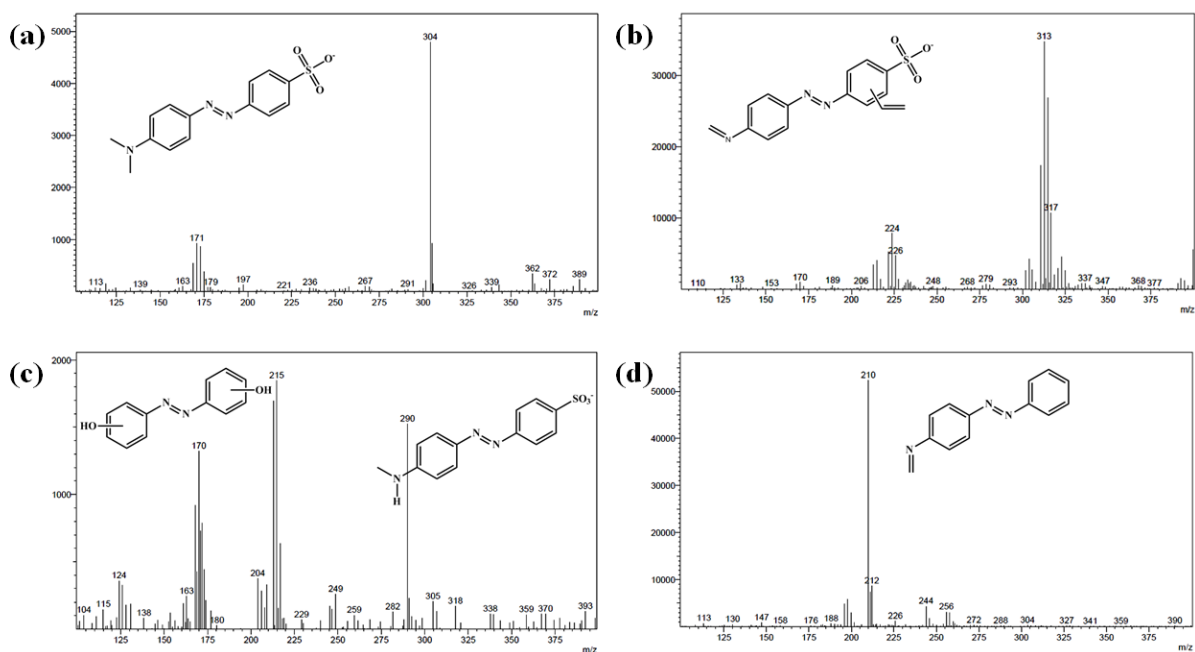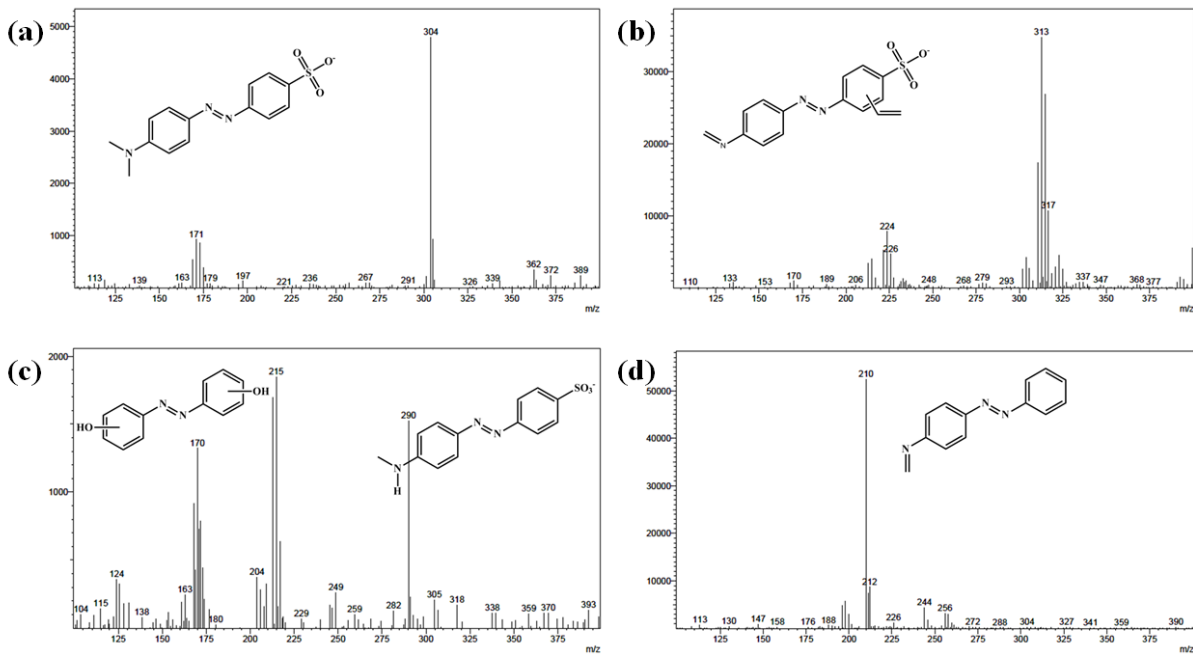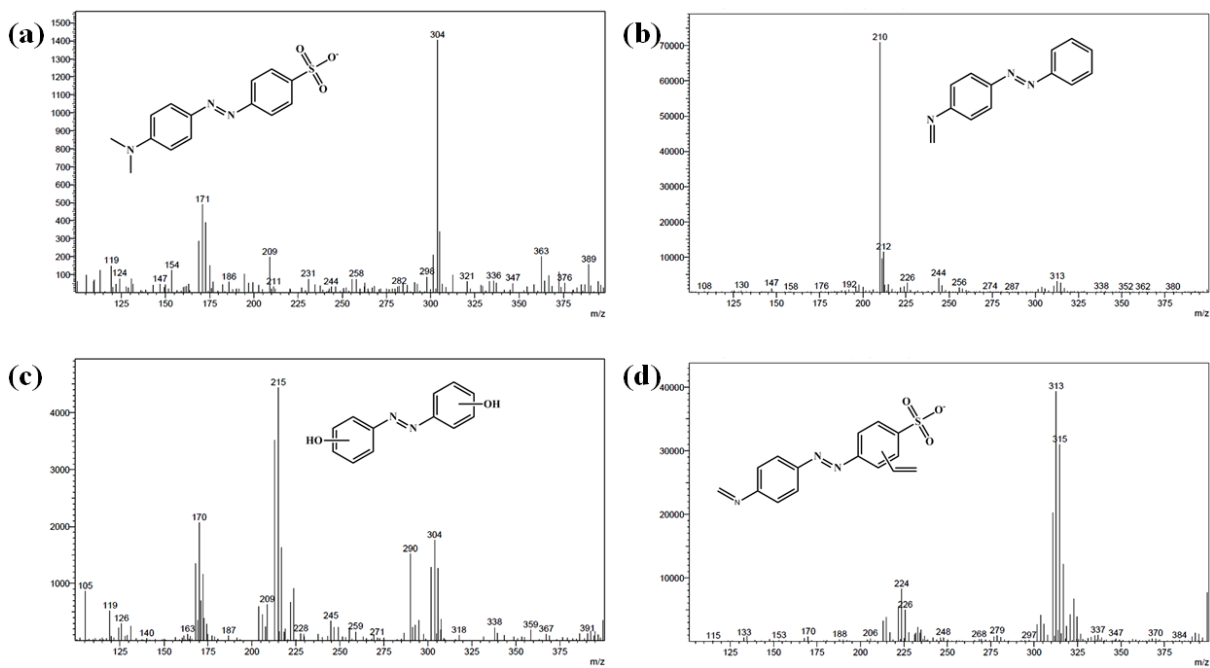
Fig. S8 Mass spectrum of initial MO solution

Fig. S9 Mass spectra of the by-products evolved by the sonophotocatalytic degradation of MO using CuO-TiO$_2$ photocatalyst at 20 min with *m/z* (a) 304 (MO), (b) 313, (c) 290 and 215, and (d) 210.

Fig. S10 Mass spectra of the by-products evolved by the sonophotocatalytic degradation of MO using CuO-TiO₂ photocatalyst at 60 min with *m/z* (a) 304 (MO), (b) 313, (c) 290 and 215, and (d) 210.

Fig. S11 Mass spectra of the by-products evolved by the sonophotocatalytic degradation of MO using CuO-TiO₂ photocatalyst at 120 min with *m/z* (a) 304 (MO), (b) 210, (c) 215 and (d) 313.
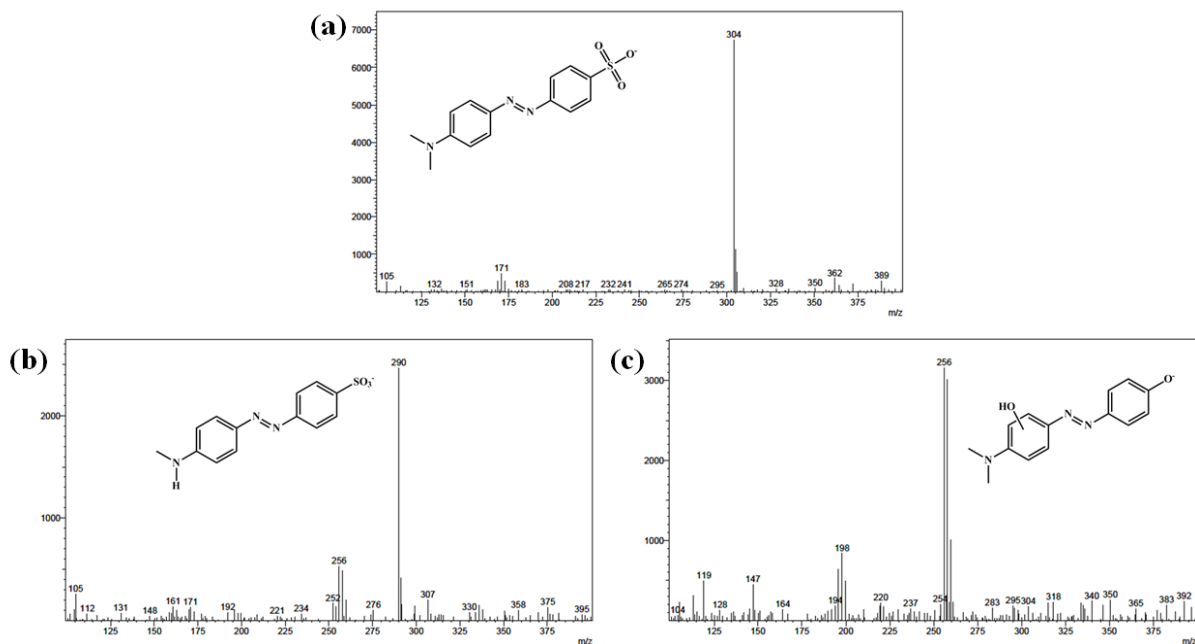
Fig. S12 Mass spectra of the by-products evolved by the sonophotocatalytic degradation of MO using CuO-TiO$_2$/rGO photocatalyst at 20 min with *m/z* (a) 304, (b) 290 and (c) 256.
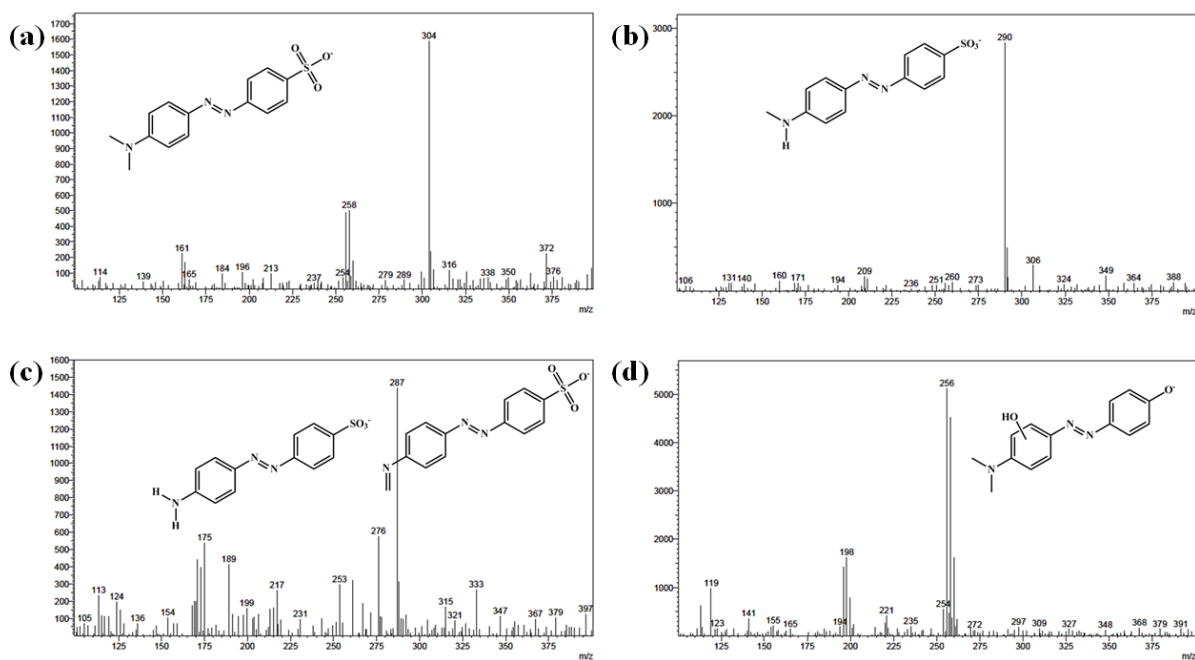

Fig. S13 Mass spectra of the by-products evolved by the sonophotocatalytic degradation of MO using CuO-TiO$_2$/rGO photocatalyst at 60 min with *m/z* (a) 304, (b) 290, (c) 287 and 276, and (d) 256.
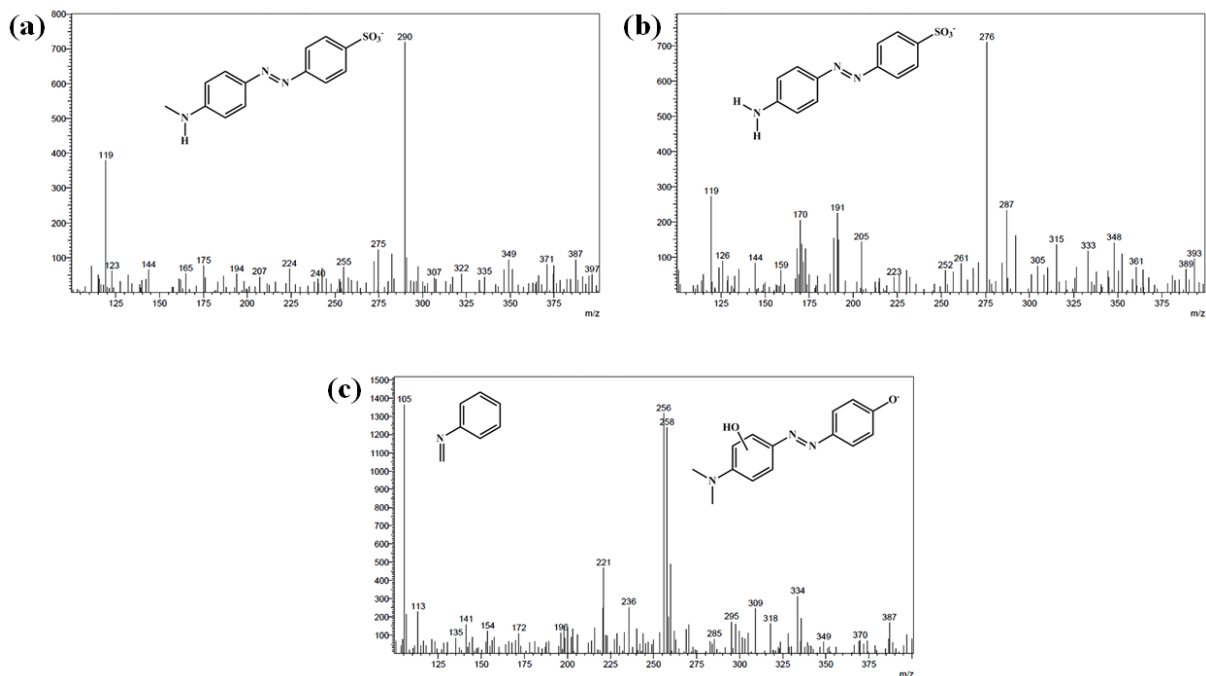
12

Fig. S14 Mass spectra of the by-products evolved by the sonophotocatalytic degradation of MO using CuO-TiO$_2$/rGO photocatalyst at 120 min with *m/z* (a) 290, (b) 276 and (c) 256 and 105.
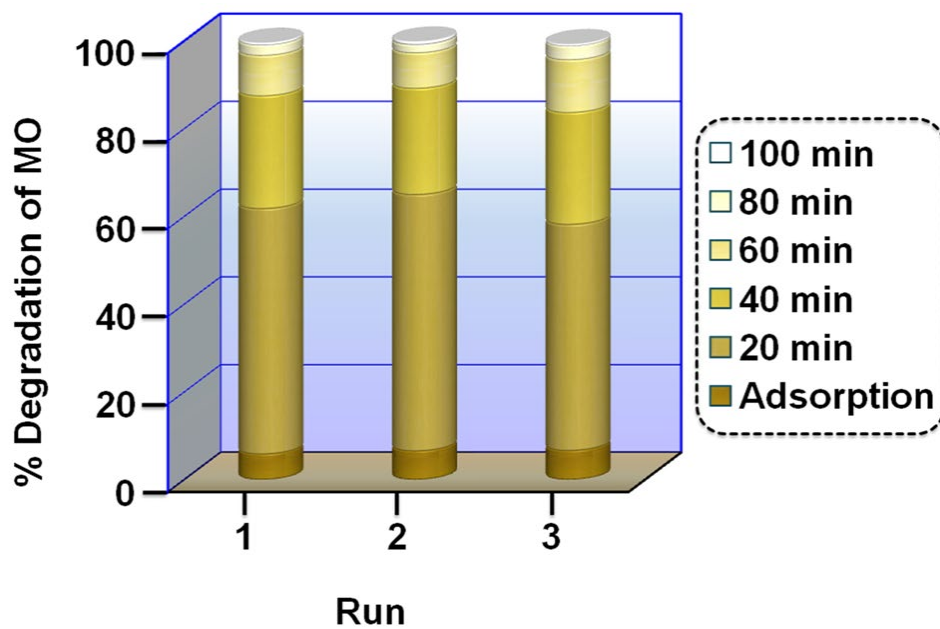

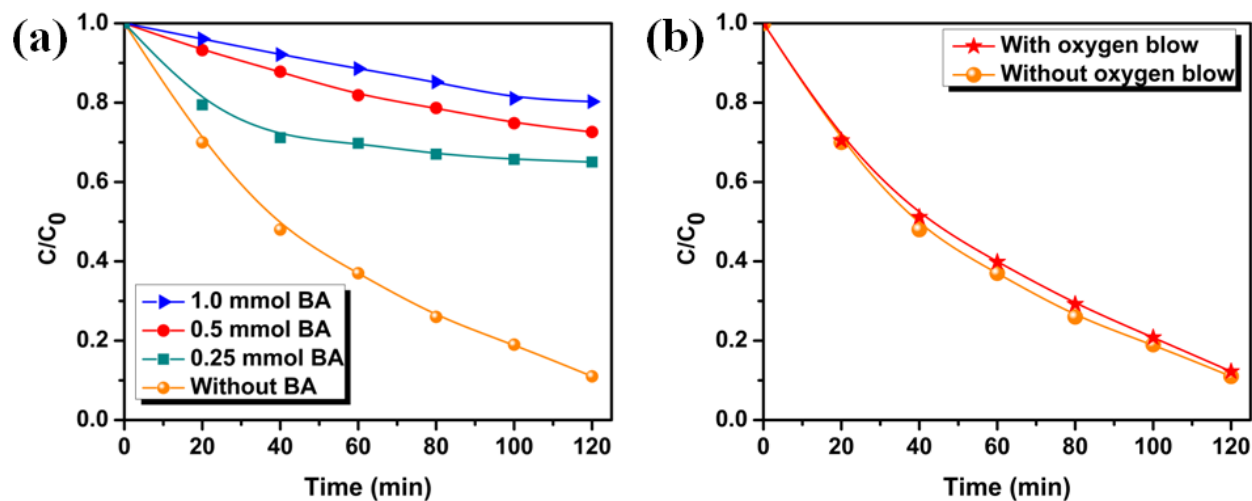**Fig. S15** Reusability tests.

13

Fig. S16 Effect of (a) benzoic acid (BA) and (b) oxygen blow in ultrasound assisted photodegradation of MO under diffused sunlight.

References

[1]   C.S. Lu, C.C. Chen, L.K. Huang, P.A. Tsai, H.F. Lai, Photocatalytic Degradation of Acridine Orange over NaBiO$_3$ Driven by Visible Light Irradiation, Catalysts 3 (2013) 501–516.

[2]   S.K. Kansal, M. Singh, D. Sud, Studies on TiO$_2$/ZnO photocatalysed degradation of lignin, J. Hazard. Mater. 153 (2008) 412–417.

[3]   Y. Abdollahi, A.H. Abdullah, U.I. Gaya, S. Ahmadzadeh, A. Zakaria, K. Shameli, Z. Zainal, H. Jahangirian, N.A. Yusof, Photocatalytic degradation of 1,4-benzoquinone in aqueous ZnO dispersions, J. Braz. Chem. Soc. 23 (2012) 236–240.

[4]   D.D. Dionysiou, A.P. Khodadoust, A.M. Kern, M.T. Suidan, I. Baudin, J.M. Laine, Continuous-mode photocatalytic degradation of chlorinated phenols and pesticides in water using a bench-scale TiO$_2$ rotating disk reactor, Appl. Catal. B: Environ. 24 (2000) 139–155.